OSLO METROPOLITAN UNIVERSITY
STORBYUNIVERSITETET

Department of Civil Engineering and Energy Technology
Institutt for Bygg- og energiteknikk
Energi og miljø i bygg

Postadresse: Postboks 4 St. Olavs plass, 0130 Oslo
Besøksadresse: Pilestredet 35, Oslo

Telefon 67 23 50 00
www.oslomet.no

Gruppe/Kandidat nr.
416

Tilgjengelighet
Open

MASTER THESIS

Title	Date
CFD analysis of human respiratory events in indoor environments	01.06.2022
	Number of pages/number of appendixes: 57/9
Authors: Oda Martine Sundsdal	Supervisor: Arnab Chaudhuri
Written/performed in collaboration with: Convergent Science GmbH, Austria	Contact person: Suresh Kumar Nambully

ABSTRACT

This work aims to explore realistic scenarios of human respiratory events in an indoor environment. A FVM based 3D based multiphase solver, with an adaptive mesh refinement function, is used to solve the compressible multi-component fluid with an Eulerian-Lagrangian approach. Since recent studies claim that particles are assumed to remain airborne with very low diameters for longer periods, this thesis combines realistic scenarios of respiratory events and incorporates a user defined function that ceases evaporation of droplets smaller than a diameter of 5 μm, together with a thermal difference between the person and the surroundings.

Key words

Computational fluid dynamics
Human respiratory events
Indoor environment

Preface

This masters thesis is the finalisation of the study program Energy and Envirnonments in buildings-sivil ingeniør at OsloMet.

I want to use this space to thank my supervisor, Arnab Chaudhuri. Thank you for all your help and support this semester, but also the last couple of years. I will continue to hear your voice messing "ikke stress Oda, ikke stress" during challenging tasks at work.

I'd like to express my gratitude to Suresh Kumar Nambully for his clarification and assistance with the model setup.

I also want to thank my fellow student and friend Ole Norbec for collaboration during the last year. It has been long discussions regarding cases, simulations and literature, but also talks about life and a trip to a random conference in France. Thanks also for constant support during periods with low motivation.

Lastly, I want to thank my fellow students, and friends, for five good years at OsloMet, all those months homeschooling included. It has been good talks about both school and life, endless hours of studying, lots of trips to Espresso House, and so much more. I'm forever grateful for all the great memories we have made.

Oda Martine Sundsdal, 01.06.2022

Abstract

The global Covid-19 pandemic has increased the interest in viral transmission of viruses. One can also argue that the same mechanisms that helped SARS-COV 2 spread so rapidly throughout the world have increased the relevance of the field. Recent studies claim that airborne transmission of viruses play an important role in the spread of viruses. The technology of computational fluid dynamics (CFD) and machine learning tools within the area of viral transmission of particles, especially viruses, have developed significantly the last years, followed by increased use of the tools.

This work aims to explore realistic scenarios of human respiratory events in an indoor environment. A FVM based 3D based multiphase solver, with an adaptive mesh refinement function, is used to solve the compressible multi-component fluid with an Eulerian-Lagrangian approach. This thesis uses realistic scenarios of respiratory events. Latest research claim that particles with very low diameters remain airborne for longer periods. Therefore, is a cut-off function of the evaporation when the droplet diameter becomes smaller than 5 μm implemented, in addition to a thermal difference between the person and the surroundings analyzis.

To investigate the respiratory events in the indoor environment, nine simulation cases are considered. The considered cases were, mainly, performed in a typical single person office with one person breathing and coughing. In addition, one simulation investigates the same office setup with two people breathing and talking. The novelty of the present works lies in the fact that a combination of realistic breathing-coughing / breathing-talking scenarios together with cut-off evaporation to resolve micro-droplets including the thermal effects were analyzed. The implementation is first verified with an elevator setup.

Then, a preliminary sensitivity analysis of two-equation turbulence models. The results show no significantly variations between the tested models, and the results are in accordance with the literature.

The results indicate that ACH variation influences the droplets in the room significantly. The results show that higher values of the ACH will disperse the droplets in the domain at a faster rate than the lover ACH. This is an interesting aspect in relation to the risk of infection spread via airborne particles and how ventilation can be used as a strategy for reduction of the spread of infection. Lastly, the implemented methods are demonstrated in a realistic scenario with two persons breathing and talking. The results highlight the connection between the thermal plume, the trajectories of the droplets and the flow filed in the computational domain.

Sammendrag

Nyere forsking peker mot at luftbåren smitte spiller en viktig rolle i spredningen av smittsome virus. Grunnet den globale pandemien Covid-19 har interessen for, og relevansen av, studier som undersøker luftbåren smittespredning økt betraktelig. Bruken av CFD- og maksinlærings verktøy innenfor området er svært relevant, og har hatt en stor økning den siste tiden.

Denne masteroppgaven utforsker hvordan dråper fra pusting, hosting og snakking i realistiske innendørs senarioer sprer seg i rommet. I oppgaven blir et avansert FVM og 3D basert simulerings program,som baserer seg på en Eulerian-Lagrangian tilnærming til hvordan spytt som eksahelses oppfører seg i gass- og væske fasen, benyttet. Forsking fra nyere tid hevder at ekshalerte partikler kan forbli luftbåerne over lengere perioder, og et av målene i oppgaven er å undersøke hvordan disse små partiklene, som forblir luftbårene, oppfører seg. For å se nærmere på dette er det lagt inn en funskjon som stopper fordampningsprosessen til en dråpe når diameteren er 5 μm eller lavere. I tillegg er det lagt inn en temperaturdifferanse mellom omgivelsene og personen i modelen, for å obervere effekten av dette.

Det er sett opp ni simuleringscaser, casene er basert på et typsik cellekontor med en person som puster og hoster. I de første fem casene varieres valg av turbulens modeller, der målet er å undersøke hvor sensitiv simuleringen er for valg av modell. I de tre neste casene varieres ventilasjonsluftmengdene i kontoret for å evaluere hvordan dråpene fra pusting og hosting sprer seg i rommet, distribusjon av dråpestørrelser og utvalgte andre parametere. Til slutt er det satt opp en case hvor en person nummer to kommer inn i rommet og står ved døren. I denne simuleringen er det lagt inn en realistisk sekvens med pusting og prating. Resultatene presenterer en sensitivitetsanalyse av de ulike turbulensmodellene. Resultatene viser få merkbare variasjoner mellom de ulike modellene, men er i samsvar med tidligere forskning. Resultatene fra simuleringene med variasjoner av luftmengdene peker mot at ulike luftmengder i stor grad vil påvirke spredningen av dråper i rommet. Høye luftmengder vil raskere spre dråpene ut over i hele rommet enn det lavere luftmengder vil. De implementerte metodene er, til slutt, demonstrert i et realistisk scenario med to personer som puster og snakker, resultatene fremhever sammenhengen mellom termiske plume, spedning av dråper og luftstrømingene i rommet.

Contents

List of Tables

List of Figures

1 Introduction

Recent claims that airborne transmission of viruses play an important role in the spread of viruses [1], [2]. Due to the ongoing global Covid-19 pandemic that we are all affected by, the interest and relevance of the viral transmission of viruses have increased considerably.

The recommendations for social distancing introduced by WHO is "much" based on the research paper by Wells and Stone where they looked at the viability of droplet infection [3].Their results show that mostly larger respiratory droplets (defined as radius > 100 μm) contains infectious pathogens, and that such droplets will remain in the breathing zone for the initial 1-2m after being ejected from the source, before being dominated by gravity and falls towards the floor. More recent studies show that smaller droplets, with diameters less than 5 μm that can remain airborne for longer periods, up to several hours, are likely to contain infectious pathogens like the virus Covid-19 [1], [2]. There are also studies that imply that these small respiratory droplets have a significant impact on the spread of infection [4], [5].

These new findings regarding the influence small respiratory airborne droplets have on the spread of infectious pathogens, can be used as a motivation for more comprehensive studies regarding the understanding of the viral transmission in indoor environments. It also implies that ventilation and ventilation strategies can be seen as one of the major strategies for reducing the spread of infections. If this strategy is to reach its full potential, we need to gain more knowledge regarding the properties of fluid flows in indoor environments, especially the behaviour of floating particles that can contain viruses. The use of computational fluid dynamics (CFD)- and machine learning tools within the area of viral transmission of particles, especially viruses, have developed significantly in the last years. Both due to the pandemic, but also due to great progress in the development of the technology.

This thesis is based on, and is an extension, of Patrick Paulsen's thesis "Analysis of human cough in confined spaces: a numerical study" from last spring [6]. Paulsen aimed to revisit the human cough instances in an elevator setup using three-dimensional adaptive mesh refinement (AMR) based computational fluid dynamics multiphase flow solver. The results from his study highlights the benefits of AMR based techniques for analysis of complex multiphase flow.

1.1 Literature review

The publication rate in this area has increased significantly the last couple of years. This is most likely due to the global pandemic, Covid-19. As mentioned in the introduction, the pandemic has clearly highlighted the importance and relevance of this research field. This section will give a brief overview over some relevant studies on viral transmission in confined spaces. First, a selection of studies dealing with numerical studies of human respiratory events will be presented, and then some experimental studies regarding the properties of exhaled droplets and thermal plumes due to temperature differences will be summarized.

Dbouk and Drikakis propose an Eulerian-Lagrangian approach to model the multiphase flow from coughing [7], where they analyse and observe the instances of a cough in a confined space. Arpino et al. propose a similar approach, where they also use the Eulerian-Lagrangian model to numerically analyse the transient and non-isothermal dispersion of aerosols in a car cabin. They aimed to develop a numerical tool that can be used for risk analysis of the potential infection risk due to viral transmission on short journeys [8]. Several cases are discussed in the article, using different HVAC systems. In addition, one case place the passenger in the front seat while another case have the passenger in the back seat. The main conclusion from the study is that the risk of spreading infection through airborne virus transmission in a short journey is strongly dependent on the HVAC system. This conclusion comes with the assumption that the risk of virus transmission from the infected person to the other person is directly related to the number of inhaled particles. Bhat et al. published a highly relevant study in March 2022 [9] where they modelled the potential airborne transmission of SARS-CoV-2 virus in a conference room. They conducted a numerical study revisiting the respiratory droplets from breathing, talking, and coughing in a room with ten people sitting around a conference table. The study uses the Navier-Stokes equations to solve the injected multiphase flow, and models the liquid phase of the droplets as discrete phase with the Lagrangian approach. Scenarios with and without air condition and face masks were considered. To analyse the transport of respiratory droplets, the discrete phase model based on experimental data from earlier studies was used. To mimic the biological flow patterns of human respiratory events, they used analytical functions. The observations in this study suggests that the spread of smaller respiratory droplets are heavily influenced by natural convection. The simulations with face mask imply that the masks significantly reduces the travel distance of the particles due to filtration and pressure drop through the mask. However they find an increase of droplets that spread in lateral direction close to the body. They conclude the study by showing the importance of a good air condition design is to reduce spread of infection through airborne transmission.

The turbulence modelling in the different studies are in most cases based on the RANS equations combined with a two-equation turbulence model. The revisited studies mentioned in this thesis mainly uses the standard and realizable k-ϵ models and the SST k-ω model. Motamedi et al. uses the realizable k-ϵ model in their CFD study regarding ventilation strategies and risk of infection [10]. And Busco et al. uses the same model in their studies of the viral transmission from sneezing with a CFD approach. There are also some studies that report valid results with the usage of the SST k-ω model in similar studies [11], [12]

Measurements and models regarding respiratory events, like mass, size, distribution, and injection duration are widely reported in the literature. This thesis does not contain its own experiments and is therefore based on findings from experimental studies. Most of the studies mentioned above are also theoretical studies that are based on findings reported in the literature. The size distribution of exhaled particles from different respiratory events has been measured and fitted into mathematical models. Several studies report that the most fitting size distribution for breathing and talking is the log-normal distribution [13]–[16]. Others suggest combinations of models, like Morawska et al.

who suggest that the most fitting model for talking events would be a combination of a gamma- and log-normal distribution [17]. On the other hand the Rosin-Rammler model have been suggested for size distribution of the droplets from coughing and sneezing [7]. Regarding the exhaled mass from respiratory events, the literature does not give an exact answer, as the different studies have quite divergent findings. This thesis is mainly based on Zhang et al. [18] and Xie et al. [19] regarding characteristics of exhaled respiratory droplets. An exhaled liquid mass of 0.033 mg for a breath (approximately 2.5 seconds) and about 1.3 mg for 3 seconds with talking are being reported. In addition, Dbouk and Drikakis report a mass of 7.7 mg of exhaled liquid for a typical cough [11]. The time intervals of human respiratory events have been reported in several studies. A typical breathing sequence that occurs in the literature are repeated cycles of 5 seconds that consists of 2.5 seconds exhaling and 2.5 seconds inhaling [20]. For talking, an example is a repeating cycle of 5 seconds with 3.5 second exhaling and 1.5 second inhaling [20]. Coughing is reported in sequences where the time of exhalation for on cough is used, Dbouk and Drikakis uses 0.12 second in their study [11]. The same studies are also reporting on the velocity of the injected particles/droplets when breathing, talking and coughing. Chao et al. reports a jet-shaped injection with an average velocity of 11.7 m/s for coughing and 3.9 m/s for talking [13]. While Zhang et al. reports that the velocity of the droplets for breathing lies between 0.1 and 1.0 m/s and between 10 and 25 m/s for a cough [18].

It can be realized that the velocity field in a domain is affected by several factors. One of the main factors are temperature differences. Several studies report increased velocity in the area above an object with higher temperature than the surroundings, e.g. a person in an indoor environment. The surface temperature of an average person is around 34°C while the typical air temperature in an indoor environment is 22°C [21], [22]. This difference leads to changes in the air velocity around the person. Several studies report an observed thermal plume above the person [22]. This plume has an increased velocity profile in the upwards direction, the magnitude is dependent on surrounding factors such as air velocity and temperature. Gao and Niu published a study where they did both measurements and CFD analysis regarding the air flow in a room with displacement ventilation [23]. With an established velocity field around 0.02 m/s in the domain they found that the velocity in the upward direction in the thermal plume will vary between 0.1 and 0.25 m/s. Sørensen and Voigt report similar findings from their CFD-analysis of the heat transfer around a human body [21]. They compare experimental data with CFD-simulations and present findings that illustrate the close connection between the temperature differences, heat convection, velocity field and the thermal plume.

1.2 Objective

The objective of this thesis is to explore realistic scenarios of human respiratory events in indoor environments, with a main focus on investigating the effects of different turbulence models, and variation in the ACH. This is done by implementing a cut-off evaporation function to cease evaporation of droplets smaller than a diameter of 5 μm which enables us to realistically investigate the dispersion of the injected droplets in the domain over time. The effect of temperature difference between the human

beings and the environment is also investigated. This is done using a three-dimensional adaptive mesh refinement-based multiphase flow solver, CONVERGE 3.0 [24].

The first part of the analysis is a sensitivity analysis of four different two-equation turbulence models with the purpose to investigate the differences between them. Then dispersion and distribution of droplets will be investigated and analysed with variations of the ACH. To create a realistic breathing-talking scenario, a simulation with two persons is implemented in the study. This work aims to add a novel approach on how to gain new knowledge and understanding of the airborne viral transmission from human respiratory events in indoor environments.

This work is structured as follows: Firstly, relevant theory regarding governing equations, turbulence models and the chosen solving tools are described. Then a description of the problem set up and the simulation cases are given in the methodology. Lastly, an analysis and discussion regarding the simulation results are given in the result and discussion chapter. Section 4 is divided into parts; a sensitivity analysis of the turbulence modelling, investigation of the properties of the fluid flow with variations in the ACH, and a brief analysis of a case with two persons breathing and speaking. The work is summarized and concluded in section 5, with suggestions for future work.

1.3 Limitations

The limitations in this thesis are briefly described in this section. The limitations are listed in the list below, with further description of the major ones given below.

- Only simulations, no experiments
- Salvia droplets are modelled as pure H_2O
- The human body is modelled by simple rectangular boxes
- The temperature of the supply air and exhaust air are set to the same temperature in the simulations.
- The base mesh dependency in case 6-8
- Time

One of the main limitations with the results in this thesis is the lack of experimental data. To be able to validate and confirm the results, further work must be done. On the other side, the results that are presented and analysed are consistent with previous studies and literature, and it can therefore be argued that the results are relevant and interesting for the understanding of viral transmission of multicomponent fluid flow in indoor environments.

The saliva droplets are modelled as pure H_2O, but in reality saliva droplets are salt solutions. This can affect both the mass of the droplets and the evaporation process, and by this also the effect of the gravity. However, the difference of H_2O and a salt solution on these very small droplets are considered to be so small that the error can be accepted.

The temperature of the supply air and exhaust air are set to the same temperature in the simulations. Due to internal heat sources in a normal office set up, this is not realistic. Due to internal heat sources in a normal office set up, the inlet temperature is normally a couple of degrees lower than the outlet temperature.

The model of the human body is a group of boxes, in further studies at least the head should be modelled more circular. Due to difficulties with the mesh and time, this was not done in this master thesis, but it should be investigated further.

The base grid in simulation case 6-8 are adjusted to save data power and time due to power issues with the HPC-facility. Since the simulations had to be done locally at OsloMet, with fewer processors than in the HPC-facility, this was necessary. Detailed mesh sensitivity analysis is not performed during this time bounded project. The solution relies on the justified near wall mesh resolution and AMR based approach to resolve the local variations of the complex flow-field.

2 Theory

This chapter gives an introduction and a brief account of the theory behind the flow physics involved in the indoor setup. The chapter is the baseline for the decisions regarding choices of different physical models, parameters and values. Firstly, it will give a description of relevant governing equations, turbulence modelling, and a few other models and considerations. Then an explanation of what computational fluid dynamics (CFD) is and how it works.

2.1 Governing equations

A multiphase fluid can be described by an Eulerian-Lagrangian specification of the properties of the fluid flow. Where the Eulerian approach is used to describe the gas phase and the Lagrangian approach for the liquid phase. The main difference between the approaches is that the Eulerian equations calculate the flow properties based on regions (small volumes) and the Lagrangian phase calculates the properties of the fluid of each particle. Both approaches have a set of governing equations that will be presented in this section.

2.1.1 Eulerian phase

The Eulerian approach is used to describe the gas phase of the fluid. The governing equations and turbulence modelling regarding this phase are described in this section. The first equation is the continuity equation that describe the mass conservation in a three-dimensional, unsteady, compressible flow. The continuity equation is presented in equation 1, where ρ represents density, $\mathbf{u}$ the velocity vector and t time.

$$\frac{\partial \rho}{\partial t} + \nabla \cdot (\rho \mathbf{u}) = 0 \tag{1}$$

The momentum of the flow is described by equation 2. This equation describes the momentum of the flow depending on the forces acting on the fluid. Where P represents pressure, μ the dynamic viscosity, S_M the source term. The source term can e.g. represent the gravity working on the fluid.

$$\frac{D(\rho \mathbf{u})}{Dt} = -\frac{\partial P}{\partial x} + \nabla \cdot (\mu \nabla \mathbf{u}) + S_M \tag{2}$$

The conservation of energy is presented in the energy equation, see equation 3. Φ is the dissipation function that contains the effects due to viscous stresses. S_i

$$\frac{\partial (\rho i)}{\partial t} + \nabla \cdot (\rho i \mathbf{u}) = -p \, \nabla \cdot \mathbf{u} + \nabla \cdot (k \, \nabla \, T) + \Phi + S_i \tag{3}$$

The ideal gas law is used to link pressure, temperature and density of a compressible multicomponent gas mixture. The equation of state is presented in 4. Where R is the specific gas constant, P is pressure, T is temperature and ρ is density.

$$P = \rho RT \tag{4}$$

2.2 Turbulence modelling

Turbulent flow can be described by characteristics, where two of the overall categories are free turbulent flows and boundary layer near solid walls. The free turbulent flows can again be divided into jet, mixing layer and wake. Figure 1 illustrates the development of velocity profile in steamwise direction for the three categories of free turbulent flows. This work is mainly focusing on the turbulence in the jets issued from the mouth (see section 4.3). When a fluid of high speed is injected into a stationary flow filed with low velocity, it will form a jet region. An example of this is when a person is breathing, speaking or coughing into an established flow field. In these circumstances can, in most cases, the turbulence of the injected flow be described as a jet. The characteristics and computation of the turbulence near solid walls will be further described in section 2.3.

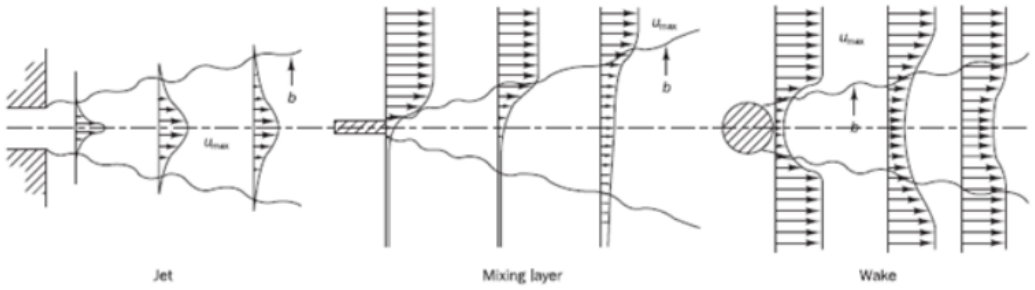

Figure 1: Illustration of velocity profiles in steamwise directions in the jet, mixing layer and wake in free turbulent flows [25]

Visualization of turbulence reveals rotational structures, called turbulent eddies. These eddies have a wide range of time and length scales that interact dynamically. To model the effects caused by turbulence there are three main numerical models; Reynolds-averaged Navier Stokes (RANS) equations, large eddy simulations and direct numerical simulation (DES). The turbulence models that are based on the RANS equations is the simplest and least time-consuming, but they are still considered to be sufficient for engineering approaches. A selection of the models that can be used to solve the RANS equations are described in more detail in the sections below.

The velocity and other flow properties in turbulent flows can be described as chaotic and random. Due to this chaotic and random pattern, turbulent flows are difficult to model. We can use Reynolds decomposition to describe the velocity and other properties in turbulent flow, see equation 5to 8.

Where U, V, W and P are steady mean values and u', v', w' and p' are fluctuating components that describe the variations from the mean values.

$$u = U + u' \tag{5}$$
$$v = V + v' \tag{6}$$
$$w = W + w' \tag{7}$$
$$p = P + p' \tag{8}$$

2.2.1 Turbulence methods for the Reynolds-Averaged Navier-Stokes equations

The turbulence models that involve the RANS equations are mainly focusing on the mean flow components and the impact the turbulence has on these components. To model the turbulence with the RANS equations equation 9, 10 and 11 must be solved.

$$\frac{\partial \bar{\rho}\tilde{U}}{\partial t} + div(\bar{\rho}\tilde{U}\tilde{\mathbf{U}}) = -\frac{\partial \bar{P}}{\partial x} + div(\mu \nabla \tilde{U}) + [-\frac{\partial\ (\overline{\bar{\rho}u'^2})}{\partial x} - \frac{\partial\ (\overline{\bar{\rho}u'v'})}{\partial y} - \frac{\partial\ (\overline{\bar{\rho}u'w'})}{\partial z} + S_{Mx} \tag{9}$$

$$\frac{\partial \bar{\rho}\tilde{V}}{\partial t} + div(\bar{\rho}\tilde{V}\tilde{\mathbf{U}}) = -\frac{\partial \bar{P}}{\partial y} + div(\mu \nabla \tilde{V}) + [-\frac{\partial\ (\overline{\bar{\rho}u'v'})}{\partial x} - \frac{\partial\ (\overline{\bar{\rho}v'^2})}{\partial y} - \frac{\partial\ (\overline{\bar{\rho}v'w'})}{\partial z} + S_{My} \tag{10}$$

$$\frac{\partial \bar{\rho}\tilde{W}}{\partial t} + div(\bar{\rho}\tilde{W}\tilde{\mathbf{U}}) = -\frac{\partial \bar{P}}{\partial z} + div(\mu \nabla \tilde{W}) + [-\frac{\partial\ (\overline{\bar{\rho}u'w'})}{\partial x} - \frac{\partial\ (\overline{\bar{\rho}v'w'})}{\partial y} - \frac{\partial\ (\overline{\bar{\rho}w'^2})}{\partial z} + S_{Mz} \tag{11}$$

Scalar transport:

$$\frac{(\partial \bar{\rho}\tilde{\phi})}{\partial t} + div(\bar{\rho}\tilde{\phi}\tilde{U}) = div(\Gamma_\phi \nabla \tilde{\phi}) + [-\frac{\partial\ (\overline{\bar{\rho}u'\phi'})}{\partial x} - \frac{\partial\ (\overline{\bar{\rho}v'\phi'})}{\partial y} - \frac{\partial\ (\overline{\bar{\rho}w'\phi'})}{\partial z}] + S_\phi \tag{12}$$

There are several turbulence models that can be implemented to solve the RANS-equations. The most used are the k-ϵ and k-ω models. The variation of the models lie in the solving of the turbulence viscosity, μ_t , in the Reynolds stresses, $-\rho\overline{u'v'}$. The relation between the Reynolds stresses and the turbulence viscosity is computed with the Boussinesq relation presented in equation 13. Four of the most used turbulence models that can be used to solve the turbulence viscosity, standard, realizable and RNG k-ϵ and SST k-ω, are described below.

$$-\rho\overline{u_i'v_j'} = \mu_t \left(\frac{\partial U_i}{\partial x_j} + \frac{\partial U_j}{\partial x_i}\right) - \frac{2}{3}\rho k \delta_{ij} = 2\mu_t S_{ij} - \frac{2}{3}\rho k \delta_{ij} \tag{13}$$

The $k-\epsilon$ models

The transport equation for the turbulent kinetic energy, k, in the considered k-ϵ models is presented in equation 14. The first term represents time, the second convection, third diffusion and the last terms are source terms. ϵ represents the scale of the turbulence. Equation 15 is the transport equation for ϵ, where the coefficients C_μ, σ_k, σ_ϵ, $C_{1\epsilon}$, and $C_{2\epsilon}$ varies between the models and are defined in table 1. σ_ϵ, marked with * in the table, requires further calculations for the realizable and RNG model, this is not displayed in detail here.

$$\frac{\partial(\rho k)}{\partial t} + div(\rho k \mathbf{U}) = div\left[\frac{\mu_t}{\sigma_k}\nabla k\right] + 2\mu_t S_{ij} \cdot S_{ij} - \rho\epsilon \tag{14}$$

$$\frac{\partial(\rho \epsilon)}{\partial t} + div(\rho \epsilon \mathbf{U}) = div\left[\frac{\mu_t}{\sigma_\epsilon}\nabla \epsilon\right] + C_{1\epsilon}\frac{\epsilon}{k}2\mu_t S_{ij} \cdot S_{ij} - C_{2\epsilon}\rho\frac{\epsilon^2}{k} \tag{15}$$

Table 1: Values for the constants in the k-ϵ turbulence models [25], [26]

	C_μ	σ_k	σ_ϵ	$C_{1\epsilon}$	$C_{2\epsilon}$
Standard k-ϵ	0.09	1.00	1.30	1.44	1.92
Realizable k-ϵ	0.09	1.00	*	1.44	1.9
RNG k-ϵ	0.0845	1.39	*	1.42	1.68

SST $k-\omega$ model

Equation 16 and 17 represents the transport equation for k and ω in the Wilcox SST k-ω model. The SST k-ω model is based on the empirical coefficients σ_k, σ_ω, γ_1, β_1, and $\beta*$, defined in table 2.

$$\frac{\partial(\rho w)}{\partial t} + \nabla \cdot (\rho k \mathbf{U}) = \nabla \cdot \left[\left(\mu + \frac{\mu_t}{\sigma_{\omega,1}}\right)\nabla\omega\right] + \gamma_2\left(2\rho S_{ij}\dot{S}_{ij} - \frac{2}{3}\rho\omega\frac{\partial U_i}{\partial x_j}\delta_{ij}\right) - \beta_2\rho\omega^2 + 2\frac{\rho}{\sigma_{\omega,2}\omega}\frac{\partial k}{\partial x_k}\frac{\partial \omega}{\partial x_k} \tag{16}$$

$$\frac{\partial(\rho\omega)}{\partial t} + div(\rho\omega\mathbf{U}) = div\left[\left(\mu + \frac{\mu_t}{\sigma_\omega}\right)\nabla\omega\right] + \gamma\left(2\rho S_{ij} \cdot S_{ij} - \frac{2}{3}\rho\omega\frac{\partial U_i}{\partial x_j}\delta_{ij}\right) - \beta_1\rho\omega^2 \tag{17}$$

Table 2: Empirical values for the constants in the SST k-ω turbulence model

	σ_k	σ_ω	γ_1	β_1	$\beta*$
Value	2.0	2.0	0.553	0.075	0.09

When the transport equations for k and ϵ or ω are solved, the turbulence viscosity can be calculated with the relation in equation 18 or 19.

$$\mu_t = C_\mu \frac{\rho k^2}{\epsilon} \tag{18}$$

$$\mu_t = \frac{\rho k}{\omega} \tag{19}$$

2.3 Near wall treatment

Solid walls interrupt the free flow pattern of a fluid. The turbulence that is created near solid walls can be categorized into three main groups, the linear sub-layer, the log-law layer and the outer layer, see figure 2. The y^+ value can be used to determine which layer the turbulence can be categorized in. y^+ can be defined as the wall coordinate: the distance y to the wall, and is made dimensionless with the friction velocity u_τ and kinematic viscosity ν, see equation 20.

$$Re_y = \frac{U_y}{v} \tag{20}$$

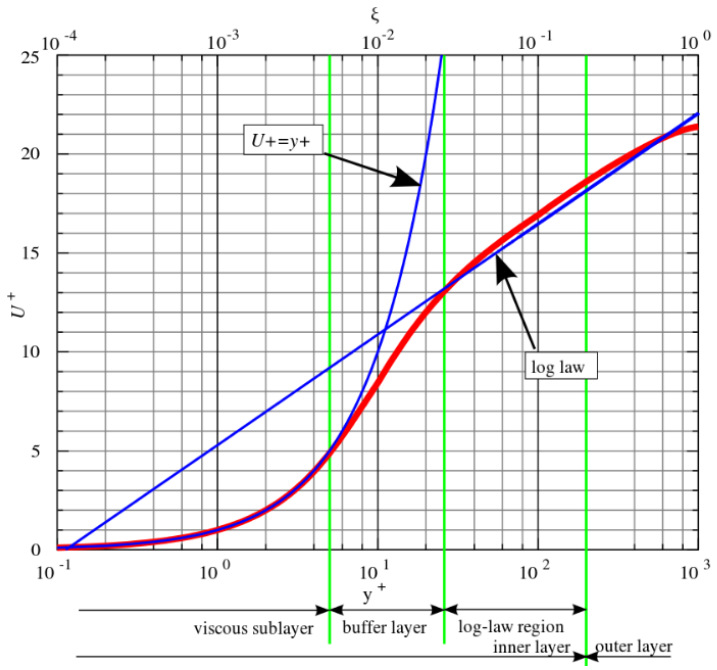

Figure 2: Illustration of the sub-layers of turbulence near solid walls [27]

2.4 Lagrangian phase

The salvia droplets are modelled with H_2O as the working fluid. The properties of the droplets are described with the equations for the Lagrangian phase, also called the discrete phase. The velocity of the droplets, v_i is modelled by the equation of motion, see equation 21. Where ρ_i represents the density of the liquid, V_d the volume of the droplet, and $F_{d,i}$ the sum of the drag force and the gravitational body force.

$$\rho_i V_d \frac{dv_i}{dt} = F_{d,i} \tag{21}$$

$$F_{d,i} = F_{drag,i} + F_{g,i} = C_D A_f \frac{\rho_g |U_i|}{2} U_i + \rho_l V_d g_i \tag{22}$$

$F_{d,i}$ is described in equation 22, where A_f represents the drop's area based on $A_f = \pi r^2$. ρ_g is the density of the gas and U_i the relative velocity between drop and gas, and is defined in equation 23, where u_i and u_i' are the local mean and turbulent fluctuating gas velocities and g_i is the gravitational acceleration. C_D is the drag coefficient, see equation 24, that is based on the drop distortion, y.

$$U_i = u_i + u_i' - v_i \tag{23}$$

$$C_D = C_{D,sphere}(1 + 2.632y) \tag{24}$$

The Frossling correlation can be used to model the evaporation of the salvia droplets [24]. The correlation is used to determine the time rate for the change in the radiuses when the droplets enter the domain. The rate is calculated by equation 25.

$$\frac{dr_0}{dt} = -\frac{\alpha_{spray}\rho_g D}{2\rho_l r_0} B_d Sh_d \tag{25}$$

$$B_d = \frac{\gamma_1^* - \gamma_1}{1 - \gamma_1^*} \tag{26}$$

$$Sh_d = (2.0 + 0.6 Re_d^{\frac{1}{2}} Sc^{\frac{1}{3}}) \frac{ln(1 + B_d)}{B_d} \tag{27}$$

$$Re_d = \frac{\rho_{gas}|U_i|d}{\mu_a ir} \tag{28}$$

$$\widehat{T} = \frac{T_{gas} + 2T_d}{3} \tag{29}$$

Apart from the above mentioned equations several other interactions should be considered for dispersed phase (liquid phase) and dispersion media (gas phase). The collision and coalescence of the droplets can be modelled by the O'Rourke collision model. This model is estimating the number of droplet collisions and their outcomes. The model is based on the thought that for a number of drops, N, the number of possible collisions of each drop is N-1 and the number of possible collision pairs is about $(1/2)N^2$. A fluid can contain an extensive number of droplets, which will make these numbers very high, and therefore result in heavy simulations. In order to reduce the computational cost, the droplets can be represented by parcels, where each parcel can contain thousands of droplets, and the collisions can be calculated based on the parcels, not each droplet. In order to reduce the cost even further, the model can use a randomly determined estimate of collisions, and in addition assume that parcels only will collide if they are located in the same fluid phase cell. The two droplet break up models Kelvin-Helmholtz model and Rayleigh-Taylor, KH-RT, can be used for modelling of droplet break-ups and instability simultaneously. With this combination the KH instability, which is based on the instabilities of the injected jet, will work alone for a given break up length, and then the RT mechanism will be activated in addition [26]. Wall interaction can be modelled with the O'Rourke film splash model. The model determines if a drop will splash or not when it hits the wall. For the drops that are determined to splash, a fraction of the drop's mass is used to create a new parcel while the rest of the mass is being incorporated to the wall [26], [28].

2.5 Mass fractions

Air at different levels of humidity contains varying fractions of O_2, N_2 and H_2O. The fraction of each component at a certain level of humidity can be calculated. The mass fractions can be calculated by, first, using Buck's equation, see equation 30, to calculate the saturated vapor pressure at a given temperature. Where T represents the temperature in $^\circ C$.

$$P_s(T) = 0.61121 exp\left[\left(18.678 - \frac{T}{234.5}\right)\left(\frac{T}{257.14 + T}\right)\right] \tag{30}$$

The vapor pressure P_v is calculated with the saturated vapor pressure and the relative humidity with equation 31. Then the vapor pressure and the room pressure (normally the atmospheric pressure) can be used to calculate the mole fraction of H_2O and the faction of air, equation32 and 33.

$$P_v = \frac{P_{sat} RH}{100} \tag{31}$$

$$\gamma_{H_2O} = \frac{P_v}{P} \tag{32}$$

$$\gamma_{air} = 1 - \gamma_{H_2O} \tag{33}$$

From here, the mole fractions and the molar masses can be used to calculate the mass fractions with equation 34.

$$\omega_i = \frac{\gamma_i M_i}{\Sigma_i \gamma_i M_i} \tag{34}$$

2.6 Computational fluid dynamics

CFD is a method of analysis based on computer-simulations of systems concerning fluid flow, heat transfer and associated phenomena. This technique is applicable in several areas, both industrial and non-industrial. In this work, CFD is applied in the analysis of air flow in indoor building-environments.

The structure of the CFD codes is based on the numerical algorithms for fluid flow problems and have three main elements; a pre-processor, a solver, and a post-processor. The part of the CFD code called pre-processing concerns the input of a flow problem to the CFD program. Sophisticated interfaces are applied in CFD programs to obtain a manageable system for the operator to insert the parameters of the problem. In the pre-processing stage there are several activities involved. The geometry of the region in question must be defined by the user. Furthermore, computational cells must be generated (known as mesh generation) and the physical phenomena that the user wishes to be considered in the analysis must be selected. At last, the fluid properties and appropriate boundary conditions between the cells and the domain must be defined. Inside each cell in the mesh there are nodes where the solution of the flow problem is defined. The accuracy of the solution, together with the cost of computer hardware and calculation time, are both a subject of the number of mesh points (computational cells). The CFD codes are constantly under development for a more adaptive mesh-generation, considering that the optimal mesh is non-uniform and has a higher degree of fineness in areas of lager variations.

After the pre-processing the next element is a solver. Most CFD codes use the numerical solution technique finite volume method (FVM). The numerical algorithm of FVM can be divided into three steps. Firstly, integration of the governing equations in the analysis, that is the fluid flow over the control volume. Secondly, the process of transforming the resulting integral equations from step one into a system of algebraic equations. Lastly, finding the solution of this set of equations, usually with an iterative method. FVM distinguishes itself from other methods and is considered desirable mostly because of the first step, the integration over a control volume. This method ensures the conservation of wanted properties in each cell in the mesh, and demonstrates the relationship between the numerical algorithm and the underlying physical conservation with FVM.

The last element in the CFD code is the post-processor. The results from the solver are being presented in the post-processor. This part is used to present the chosen data in a meaningful and interesting way. There are several ways to do this, and the results can be illustrated in numerous ways e.g. with vector or velocity plots, particle tracing, both 2D and 3D plots, even animations and further on.The presentation tools are under constant development, and are truly helpful in analysis of fluid dynamics.

2.6.1 The PISO algorithm

The PISO, Pressure Implicit with Splitting of Operators, algorithm is used to solve the Navier-Stokes equations. The algorithm is built on three steps, one predictor step and two corrector steps [25]. The algorithm starts with solving the momentum equation in the predictor step. Then the pressure is being derived and solved, which leads to a correction that can be applied to the momentum equation. After the momentum predictor and first corrector step are completed, the rest of the transport equations are solved. This sequence will be repeated in a loop util the desired accuracy is achieved [26].

3 Method

The objective of this thesis is to investigate the dynamics of respiratory droplets in an indoor environment towards the understanding of the viral transmission. This is done by making a model of a simple, but realistic, office set up and thereby perform CFD simulations with a chosen CFD software on this setup. This chapter describes the methods behind the simulations.

3.1 Problem setup

To investigate the respiratory events in the indoor environment, nine simulation cases were considered. The considered cases were, mainly, performed on a typical single person office with one person that is breathing and coughing. In addition, one simulation in the same office setup, with two persons breathing and talking was investigated. The cases can be divided into three main categories: A sensitivity analysis of turbulence models, effects on the transmission from breathing and coughing with varying ACH in the room and lastly one case with two persons that are talking and breathing. An overview of the cases is presented in table 3, and a short description of each category is given below. The geometry of the office and the persons and their properties will be described further down in this chapter.

Table 3: Simulation cases

Name	**Case description**	**Time**
Case 1	Realizable k-ϵ	10 s
Case 2	Standard k-ϵ	10 s
Case 3	RNG k-ϵ	10 s
Case 4	SST k-ω	10 s
Case 5	Realizable k-ϵ, with buoyancy effects	10 s
Case 6	Velocity supply air = 0.1 m/s, realizable k-ϵ	120 s
Case 7	Velocity supply air = 0.2 m/s, realizable k-ϵ	120 s
Case 8	Velocity supply air = 0.5 m/s, realizable k-ϵ	120 s
Case 9	Two persons, talking, realizable k-ϵ	120 s

To simulate the respiratory events, breathing-, coughing-, and talking sequences were designed. The velocity of the gas- and liquid phase of the injected spray from the three considered respiratory events are based on previous literature. The velocity in the breathing-coughing sequence for the simulations with one person is illustrated in figure 3. The velocity of the breathing sequence for person 1 and the speaking-breathing sequence for person 2 in case 9 are illustrated in figure 4.

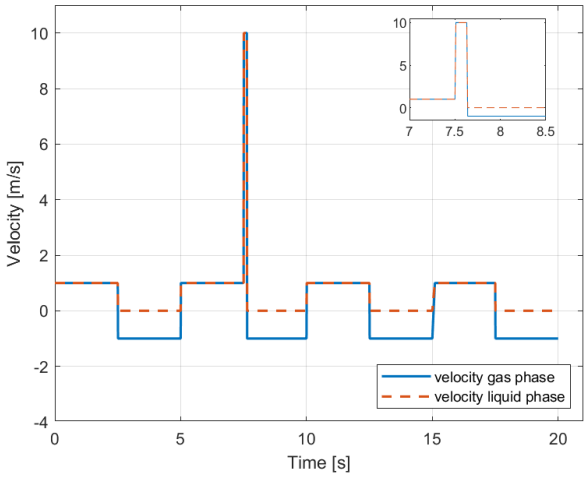

Figure 3: Velocity profile for the gas and liquid phase

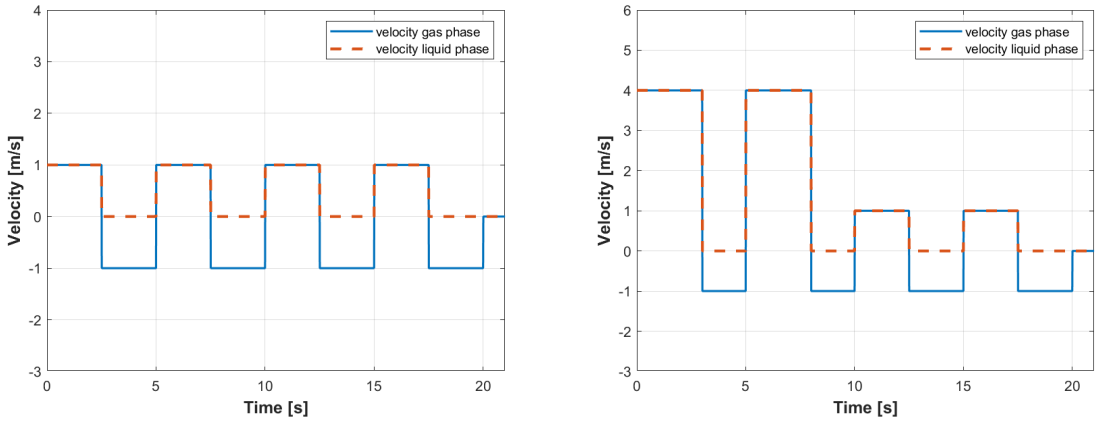

(a) Person 1, sitting person *(b) Person 2, standing person*

Figure 4: Velocity for gas and liquid phase for person one and two in case 9

The first five cases are performed with the purpose of conducting a sensitivity analysis of four different two-equation turbulence models. The considered models are the standard, realizable and RNG k-ϵ models and the SST k-ω model. The simulation time in these simulations were set to 10 seconds, and therefore is only the first 10 seconds of the breathing-coughing sequence from figure 3 used.

Case number 6-8 are simulated with variation of the ACH. With the purpose of investigating the dispersion of droplets in the domain. The air supply in case number 6 is based on the Norwegian standard for air supply. The level of air supply in case number 7 and 8 are increased to investigate the effects the air flow rate has on the particle distribution in indoor environments. These situations are

simulated for 2 minutes, and the velocity profile for breathing-from figure 3 is implemented.

Even though the simulation time is 2 minutes, the velocity is set to zero for both gas and liquid phase after 20 seconds. The reason for this is the aim to investigate how the particles are spreading in the room, and this works aims to see where the particles from the first breaths are after 120 seconds without the interference of the "newer" particles.

Case number 9 is the last simulation case. This case is based on a realistic scenario where another person is entering the office and stands in the door opening, while the person by the desk is turning towards the door. The person by the desk is defined as person 1 and the person by the door as person 2. The breathing sequence for person 1 and speaking-breathing sequence for person 2 are displayed in figure 4. The simulation time is set to 2 minutes, and the velocity for breathing and speaking are set to zero after 20 seconds in this simulation as well.

3.2 Geometry

The simulations are performed on a typical single person office setup. The office is 3 m wide, 4 m long, and 3 m high. In the geometry for case 1-8 the person is sitting by the desk, facing the wall. In the second set up, used in case 9, person 1 is sitting by the desk, facing the door, and person 2 is standing by the door, facing person 1. The dimensions of the geometry are all listed in table 4 and illustrated in figure 5 and 6.

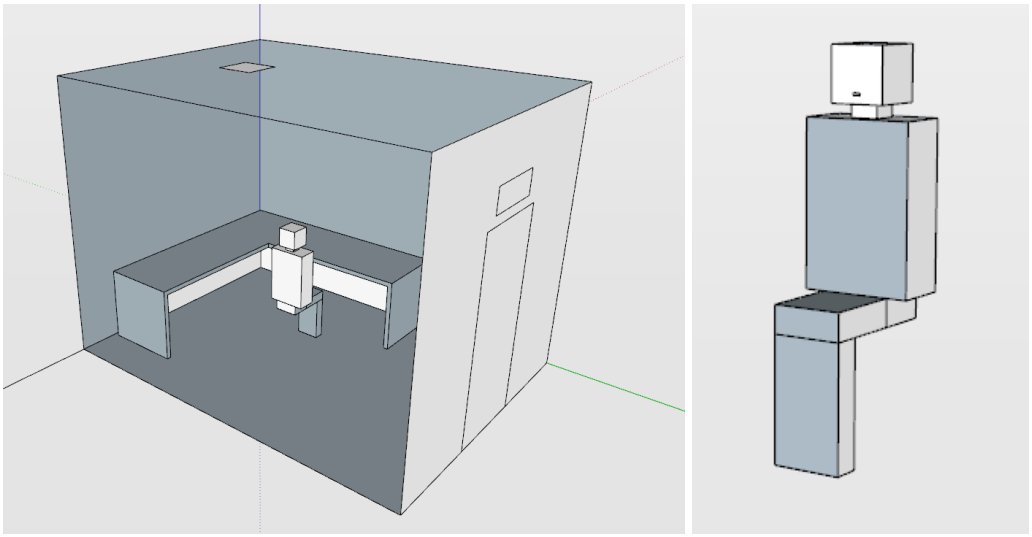

Figure 5: Illustration of the geometry used in case 1-8

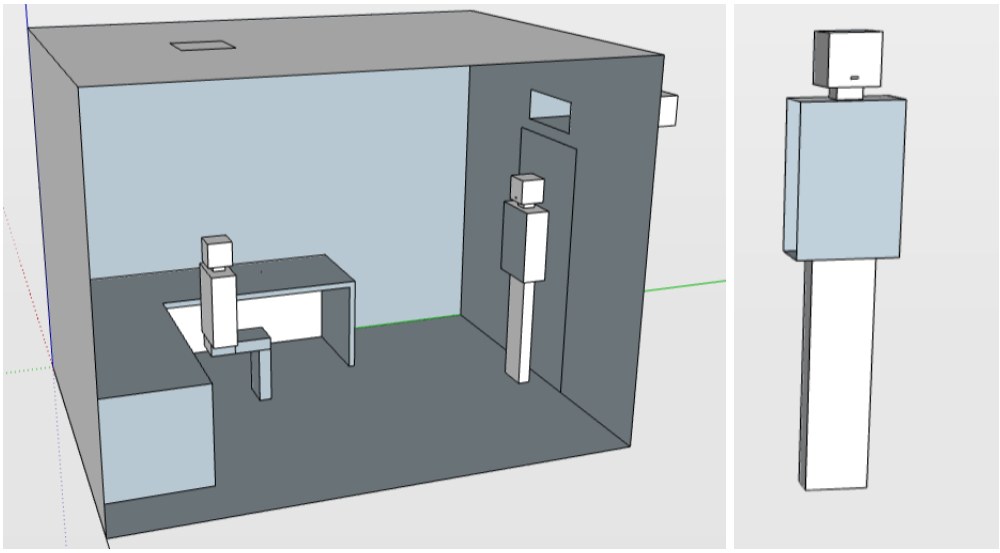

Figure 6: Illustration of the geometry used in case 9

The human geometry is simplified to make the mesh in the CFD calculations simpler. The body consist of rectangular boxes in different sizes that represent the legs, upper body, neck and head, see table 4 for measures. The rectangular boxes are placed on top of each other, and the areas of the boxes that are touching another cube, and not the surrounding air, are subtracted from the surface area of each part. The person has a height of 1.8 m and a total surface area of 1.8 m^2, in accordance with the average value for a typical Scandinavian human being [29]. When the person is sitting by a desk, the modelled height of the person is 1.4 m. Based on previous literature, the mouth is represented by a rectangle with dimensions 8.5 cm x 0.27 cm.

The size of the in- and outlet channels for air supply are calculated based on the flow rate of the air supply to make sure that the velocity in and out of the room is in accordance with the building regulations in Norway [30], regarding unpleasant draft from the supply air and disturbing sound levels from the ventilation components. The chosen measurements result in a velocity of 0.1 m/s through the inlet. The in- and outlet channels are modelled with different shapes, but with the same surface area. In the early stage of the test cases, a backflow near the outlet was observed. This backflow seamed to affect the flow pattern in the room. Therefore, a 1 meter long duct was added to account for this, to ensure that the backflow does not affect the domain of interest but instead is moved to the duct, see figure 5. This did not eliminate the backflow, but it moved the backflow from the room and into the duck.

Table 4: Relevant dimensions regarding the geometry

	Dimensions	**Total**
Room	3 m × 4 m × 3 m	36 m^3
Area air supply	0.4 m × 0.4 m	0.16 m^2
Area air exhaust	0.25 m × 0.65 m	0.16 m^2
Human height		1.8 m
Sitting human height		1.4 m
Surface area head	0.2 m × 0.2 m × 0.2 m	0.23 m^3
Surface area neck	0.1 m × 0.1 m × 0.05 m	0.02 m^3
Surface area upper body	0.4 m × 0.2 m × 0.6 m	0.85 m^3
Surface area legs	0.25 m × 0.1 m × 0.9 5 m	0.96 m^3
Surface area human		1.8 m^2
Mouth area	2.7 cm × 0.85 cm	2.3 cm^2

The geometry is made in a program called SketchUp, from TRIMBLE [31]. This is a modelling program used for drawing 3D models. The file was saved as a stl-file and imported in to the CFD simulation tool for further work.

3.2.1 Base gird and fixed embedding

For the base grid, the length, with and height, dx, dy and dz, are set to 0.15 m^2 in the case 1-5 and 9, and 0.25 m^2 in case 6-8. This sizing of the base grid results in 10 570 cells of 0.0034 m^3 and 2283 cells of 0.016 m^3 within the domain. The larger volume of the cells in case 6-8 were implemented to decrease the simulation-time.

Fixed embedding is used near the boundaries, where a finer resolution is necessary for the accuracy of the results. The walls, desk and person is scaled 2 to 1, so it is a finer grid near all the walls (the desk, human, roof and walls are defined as walls in the boundary conditions). Around the mouth the grid is even finer with a scaling of 10 to 5, see figure 7 for illustration of the base grid and fixed embedding.

In addition to the base grid and fixed embedding, an adaptive mesh refinement (AMR) function is used for the discrete phase. This function automatically refines the mesh where we have the most significant change in velocity. For the simulations in this thesis, the AMR will make a finer mesh around the spray from the breathing, coughing and talking. This function allows us to have fewer cells in the base grid, but still contain a fine grid in the area of interest, enabling us to save both time and computing power.

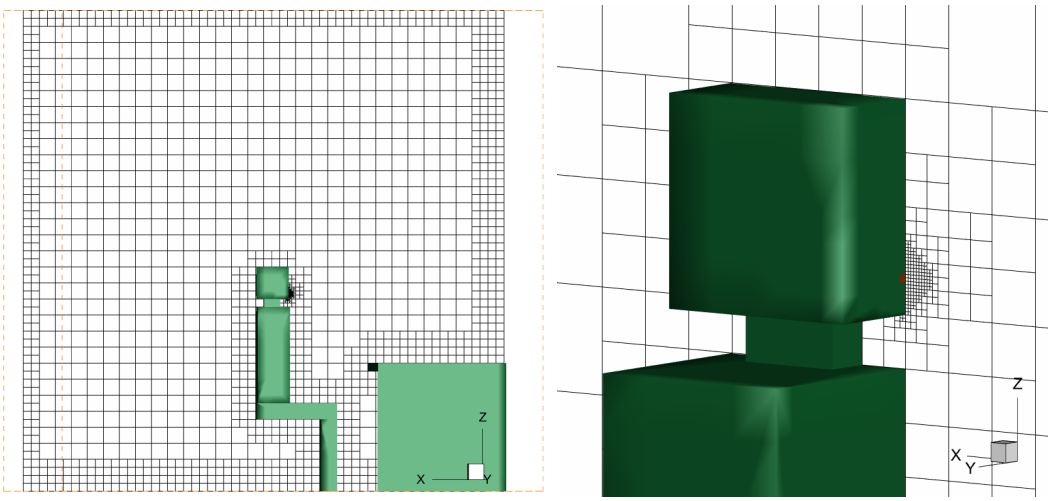

Figure 7: Illustation of the embedding in the room and around the mouth

3.3 Steady state simulations

The main simulations in this thesis are unsteady flow situations where the purpose is to analyse how an established flow pattern in an indoor environment is being affected by changes, like breathing, coughing or speaking, in the airflow. An established flow pattern is therefore desired as initial data for the transient simulations. A steady state simulation is performed to establish the flow-pattern for each case. The simulations were performed with the criteria of minium 500 cycles, and a relative tolerance of 0.0001 and maximum standard derivation of 0.01 for the mass flow rate.

The case set up in the steady and transient simulations are the same, with exception of the spray modelling. The spray from respiratory events is not included in the steady simulation. Due to this, the boundary type of the mouth is specified as a wall instead of an inlet. The spray modelling and the specifications of the boundaries will be described in more detail in section 3.6 and 3.4.

3.4 Boundary conditions

The surfaces in the computational domain are assigned to boundaries with different properties. Table 5 contains a list of which boundary type the different parts of the geometry are assigned too and information regarding essential conditions for each boundary type.

Table 5: Boundary types

Geometry part	**Boundary type**	**Specified boundary condition**
Walls, roof, desk, floor	Wall	Heat flux = 0
Inlet air supply	Inlet	$v_{airsupply}$ = 0.1 m/s
Outlet air exhaust	Outflow	P = 101325.0 Pa
Human	Wall	T = 305 K
Mouth, steady	Wall	Heat flux = 0
Mouth, transient	Inlet	Defined velocity profile, T = 307 K

3.4.1 Length scale and turbulence intensity

The length scale and turbulence intensity have been calculated and used to assign the boundary conditions for two-equation turbulence models. Equation 37 and 38 have been used to calculate these values for the ventilation inlet and the mouth. The Reynolds numbers in the calculation are based on the hydraulic diameter of the inlet and mouth, shown in equation 35.

$$Re = \frac{\rho v d_h}{\mu} \tag{35}$$

Calculation of the hydraulic diameter for the inlet is 0.4 m and is calculated for the mouth in equation 36. The hydraulic diameter is inserted as the length, L, in equation 38.

$$d_{h,mouth} = \frac{2 \cdot l \cdot b}{l + b} = \frac{2 \cdot 0.0085 \cdot 0.027}{0.0085 + 0.027} = 0.013m \tag{36}$$

$$T_i = 0.16 Re^{-1/8} \tag{37}$$

$$l = 0.07L \tag{38}$$

The calculations result in a turbulence intensity of 0.060 for the inlet, 0.052 for the mouth for talking, 0.038 for the mouth for coughing and 0.043 for the mouth for speaking. And a length scale of 0.0009 for the mouth for breathing, coughing and talking and 0.028 for the inlet.

3.4.2 Air supply

The values for air supply are based on the criteria in §13.1 in TEK 17 (the Norwegian building regulations)[30]. The demand for supply air is 2.5 m^3/h per m^2 in addition to 26 m^3/h per person. The case office has a floor area of 12 m^2 and are dimensioned for one person. This results in a demand of 56 m^3/h, which gives an ACH value of 1.6. See table 6 for calculation of the velocity boundary condition for the inlet.

Table 6: Calculation of air velocity and ACH for the supply air

	Value	**Calculation**
Inlet area	0.16 m^2	
Air supply	56 m^3/h	$\dot{V} = (2.5(m^3/hm^2) \times 12m^2) + 26(m^3/h)$
Air velocity	0.1 m/s	$v = (56(m^3/h) \times (1h/3600s))/(0.16m^2)$
ACH	1.6 /h	$ACH = 56(m^3/h)/36m^3$
Air velocity	0.2 m/s	for case 7
ACH	3.2 /h	$ACH = 115(m^3/h)/36m^3$
Air velocity	0.5 m/s	for case 8
ACH	8.0 /h	$ACH = 288(m^3/h)/36m^3$

3.4.3 Mass fractions

In the boundary conditions for the boundary types that include airflows, the mass fractions of the components in the air should be implemented. The equations from section 2.5 are used to calculate the mass fractions for air at 22°C and a relative humidity of 50 %. In this thesis, the components of air are simplified to only include oxygen, nitrogen and water vapor. The molar mass of dry air (O_2 and N_2) is 28.965 g/mole and H_2O is 18.015 g/mole. The calculations result in a mass fraction of 0.008156 for H_2O, 0.2311 for O_2 and 0.7604 for N_2. See appendix A for the full calculation.

The properties of the air in the spray are simplified to only consist of dry air and liquid spray. The factions of N_2 and O_2 for the dry air are calculated the same way as for the supply air. This results in a fraction of 0.767 for N_2 and 0.233 for O_2.

3.4.4 Mouth - boundary conditions

Figure 3 illustrates the velocity profile for both the gas and liquid phase of the respiratory events. The profile for the gas phase is added as a boundary condition for the moth. The gas phase has positive and negative values for exhalation and inhalation of air.

3.5 Turbulence modelling

The RANS equations are used for the turbulence modelling in the simulations. Together with the O'Rourke and Amsden wall heat transfer model and standard wall function for the near wall treatment. Four different two-equation turbulence models are used in the simulations. The standard, realizable and RNG k-ϵ models and the SST k-ω model. The transport equations for the turbulent kinetic energy k and dissipation rate are described in section 2.2.1. The values from table 2 and 1 are used as input data for the turbulence modelling.

As a default in the simulation program the buoyancy effects in the k-ϵ and k- models are not considered, it is therefore conducted an extra case (case 5) where the buoyancy effects were included together with the realizable k-ϵ model to analyse the sensitivity of these effects.

3.6 Spray modelling

The multiphase flow from breathing, coughing and talking are modelled as spray through a fictional injector and nozzle, illustrated in figure 8. The three different instances are modelled separately with individual injectors, nozzles and input data. This section will give a description of the spray modelling.

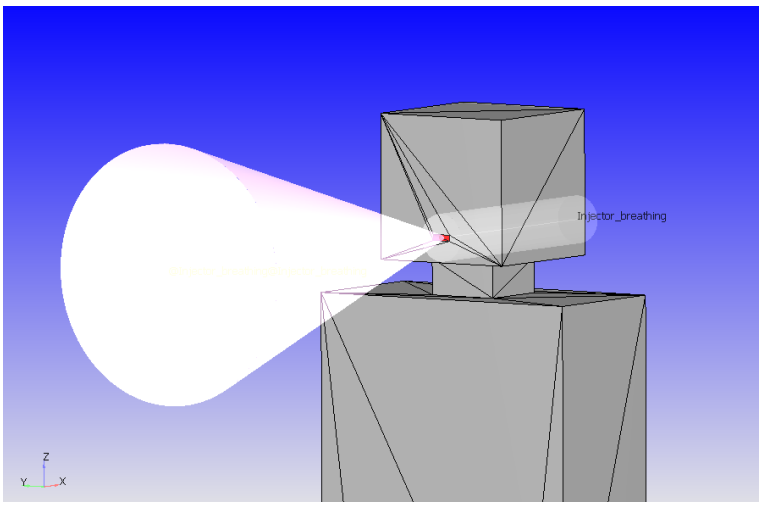

Figure 8: Illustration of the injector and nozzle

The velocity profiles for breathing, coughing and speaking in the simulation cases are defined in figure 3 and 4. The spray modelling is used to model the liquid phase of the injection. The next paragraphs will describe the properties of the injected liquid.

The injected spray is defined by signals of time and velocity. A typical breathing sequence can be defined by 2.5 second of exhaling followed by 2.5 second inhaling [20]. This 5 second sequence is

repetitive. The exhaled velocity for breathing is set to 1 m/s [18]. In this model one breath contains approximately 1600 parcels, has a mass of 0.033 mg [19] and a spray cone angle of 30 degrees [18]. A cough is modelled to last 0.12 seconds [7], with an injected mass of 7.7 mg and 3500 parcels. The spray cone angle is set to 40 degrees. For speaking, the sequence can be defined by 3.5 seconds of exhaling followed by 1.5 seconds inhaling. This 5 second sequence is repetitive. The exhaled velocity for speaking is set to 4 m/s [20]. In this model, one speaking sequence contains approximately 1500 parcels, has a mass of 1.3 mg and a spray cone angle of 30 degrees.

3.6.1 Nozzle diameter

The nozzle diameters are calculated based on velocity (v), total injected mass (m), injection duration (Δt) and density (ρ), see equation 39. The nozzle diameter for the breathing, coughing and talking sequences are calculated separately based on the values summarized in table 7. The calculations result in a nozzle diameter of 4.06×10^{-6} m, 8.95×10^{-5} m and 1.17×10^{-6} m for breathing, coughing, and talking respectively, see appendix B for the calculations.

$$d_{nozzle} = \sqrt{\frac{4m}{\rho v \Delta t \pi}} \tag{39}$$

3.6.2 Droplet size distribution

Based on the literature, the log-normal droplet size distribution is chosen for the breathing and talking sequences and the Rosin-Rammler distribution for the coughing [14], [15]. For breathing and talking the mean diameter is set to 5 μm, sigma (the standard derivation) to 0.5 and the diameter size range from 0.3 to 15 μm. The probability density function (PDF) and cumulative distribution function (CDF) for breathing are plotted in figure 9. The log normal function that can be derived from the chosen values is implemented as a user defined function under the injector drop distribution for the injectors for breathing and talking.

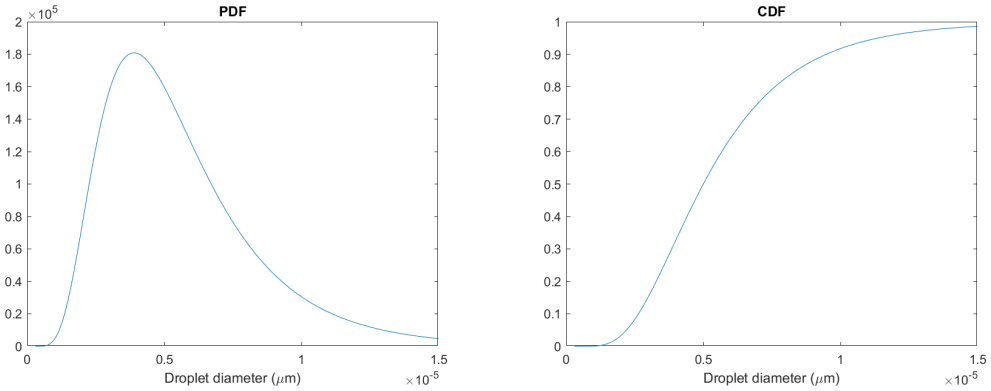

Figure 9: Distribution of the particles for breathing

The Rosin-Rammler distribution is selected for the cough. The calculation of the sauter mean diameter (smd) is calculated with a gamma function. The Rosin Rammler parameter, n, is set to 8, and the droplet diameter, d_p to 80 μm [11]. The calculation results in a smd of 73 μm, see appendix C for the calculation.

3.6.3 Evaporation

The temperatures of the droplets is assumed to be 307 K and uniform, and the evaporation model that is chosen for the simulation is the Frossling model. As mentioned in the introduction, this work aims to investigate the small airborne particles. If a normal evaporation model is used, the small droplets potentially carrying infectious virus and can be a source of infection will evaporate and disappear from the simulations. It is therefore added a user defined function that cuts off the evaporation when the droplet diameter reach 5 μm or less.

3.7 Input data

Table 7 gives a full overview over the selected values for the geometry, boundary conditions and spray modelling.

Table 7: Input data

Parameters	**Value**	**Unit**
Air supply	56	m^3/h
RH	50	%
Density	1019.32	kg/m^3
Breathing		
Mass	0.033	mg
Velocity	1.0	m/s
Parcels	1600	
Distribution model - particle size	Log-Normal	
Mean diameter	5	μm
Standard derivation	0.5	
Diameter size range	0.3-15.0	μm
Spray cone angle	30	°
Cough		
Mass	7.7	mg
Velocity	10	m/s
Parcels	3500	
Distribution model - particle size	Rosin-Rammler	
Rosin-Rammler parameter	8	
Droplet diameter	80	μm
Spray cone angle	40	°
Speaking		
Mass	1.3	mg
Velocity	4.0	m/s
Parcels	1500	
Distribution model - particle size	Log-Normal	
Mean diameter	5	μm
Standard derivation	0.5	
Diameter size range	0.3-15.0	μm
Spray cone angle	30	°

3.8 Converge

The simulations were done with the software Converge. Converge is a CFD software developed by the company Convergent Science [24]. One of the main advantages with the program is the autonomous meshing function, which is a huge benefit in the pre-processing part in a CFD code. The post-processing were done in Tecplot, which is the post-processing program from Convergent Science, and Matlab.

Table 8 contains a list with the different solving models that are chosen for the simulations in Converge Studios. The relevant theory regarding the models is described in the theory chapter.

Table 8: Solving tools in Converge

Solver	Navier-Stokes
Navier-Stokes solver scheme	PISO
Turbulence model	RANS, and standard, realizable and RNG k-ϵ and k-ω SST
Near wall treatment	Standard wall function
Evaporation model	Frossling and cut of function
Collision model	O'Rourke collision
Film splash model	O'Rourke
Injection model	Kelvin-Helmholtz and Rayleigh-Taylor
Particle size distribution of the liquid phase model	Rosin-Rammler and Log-normal
Wall heat transfer model	O'Rourke and Amsden

3.9 High performance computing

CFD simulations can be rather big and complex, and therefore consume large amounts of both data power and time. To save time, the simulations in this project have been sent to a high performance computing facility, HPC facility. The supercomputing facility that was utilised in this work is the Fram computer cluster (UiT Arctic University of Norway). The access to the Fram computer cluster was given through the project NN8005K at Notur, UNINETT Sigma2 AS (National infrastructure for scientific computational science in Norway).

The program Secure Shell Client was used to send and receive files from the HPC facility. The communication with the super computer was done through sbatch-files where case names, time estimations, placement of folder with input files, placement of folder for storage of results and number of nodes and tasks were defined in the file. An example of a typical sbatch-file from this work can be found in appendix F.

There were done some test cases in the early stage of the project that were used to finalise the setup, the information regarding consumption of cpu hours from these simulations were used to estimate the

necessary amount of data power for the final simulations. The estimations of necessary cpu hours were used to check that the planed simulations were within the limit of cpu hours assigned to the project NN8005K. See attachment E for information about both estimation and usage of nodes, processors, consumption of cpu hours and time.

3.10 Verification of the CFD model

The model used in this thesis has been tested in a similar geometry as Paulsen used in his work [6]. A short description of the setup and results of the validation case will be described here.

3.10.1 Case set up, elevator model

The simulations were performed in an elevator setup with one person. The elevator is considered a confined space with an inlet and outlet for ventilation. The geometry is illustrated in figure 10. The dimensions of the floor are 2.5 m x 1.5 m, the room is 2.4 m high, the area of the inlet and outlet are 1.0 m^2. The person is 1.75 high, has a surface area of 1.9 m^2 and a mouth modelled as a rectangle with dimensions 2.8 cm x 0.88 cm. The air supply has a velocity of 0.15 m/s and the relative humidity is set to 50 %.

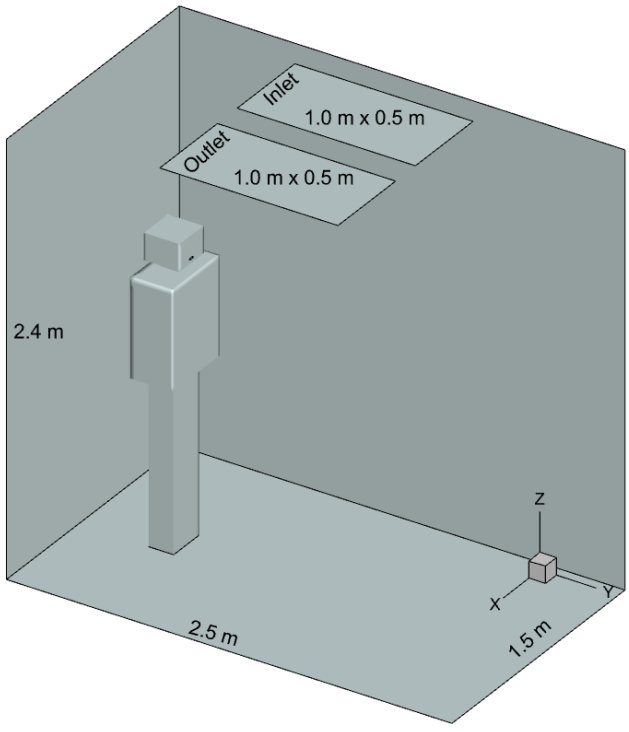

Figure 10: Geometry, elevator setup

The choices regarding the physics are the same as described for this thesis, with one main difference. For the boundary condition for the temperature of the person, the heat flux is set to zero. The turbulence model that is used is the realizable k-ϵ model, and the UDF regarding the droplet evaporation is also added in this case. The velocity for the gas and liquid phase regarding the breathing and coughing sequence is the same as in figure 10, a 20 seconds sequence that consists of four cycles of 2.5 s exhalation and 2.5 s and a single cough (0.12s) after 7.5 s.

3.10.2 Results, elevator setup

The plots in figure 11 are based on the output files from the simulation. The injected mass in plot a and b is corresponding to the defined input values regarding mass and time. Plot c is displaying the total amount of parcels in the room.

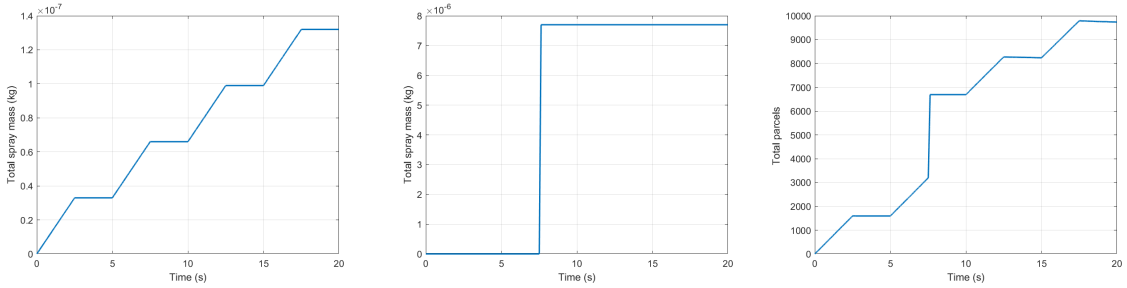

(a) Injected mass breathing *(b) Injected mass cough* *(c) Total parcels*

Figure 11: Plots from the spray output file from the validation case

The smd value reaches approximately 85 μm right after the cough. This is notably higher than the defined value of 73 μm. The higher value can be explained by the collision and coalescence model, this model assumes that some droplets will merge together and with this increase the radius of the effected droplets, and thereby increase the smd in the domain.

The wall film accumulation for the floor is plotted in plot b figure 12, and for the wall on the left and right side of the person and the person are plotted in plot c. The wall behind and in front and the roof are not plotted due to no film accumulation on these boundaries. The floor is accumulating the most particles, around 5.8 mg. With a longer simulation time, one can assume that the boundaries would accumulate more of the injected liquid spray. This would be interesting to investigate further in new studies.

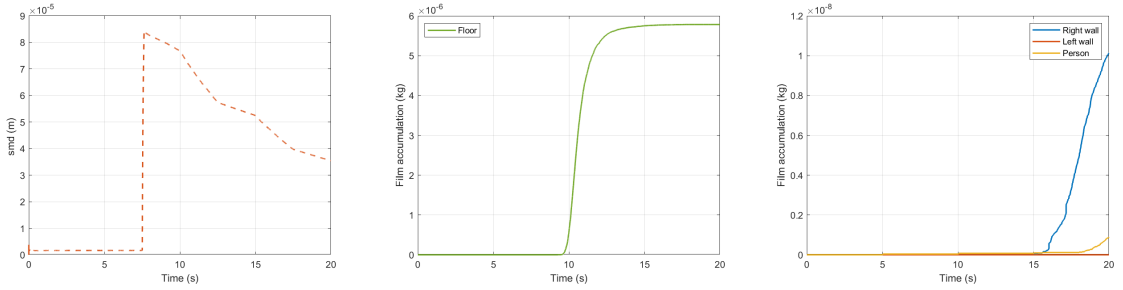

(a) Smd *(b) Film accumulation* *(c) Film accumulation*

Figure 12: Plotted smd and wall film accumulation for the wall on the left and right side of the person, verification case

Figure 13 illustrates the particle size after a breath followed by a cough. The droplets are coloured by droplet size, as can be observed the particles from the cough are significantly larger than the once from breathing. This size difference leads to different flow patterns for the particles that are entering the domain. The breathing particles have low velocity and radii and are therefore following the already existing flow pattern in the room, while the larger cough particles with a high velocity (10m/s) are injected and when the velocity decreases the droplets are being dragged towards the floor due to gravity.

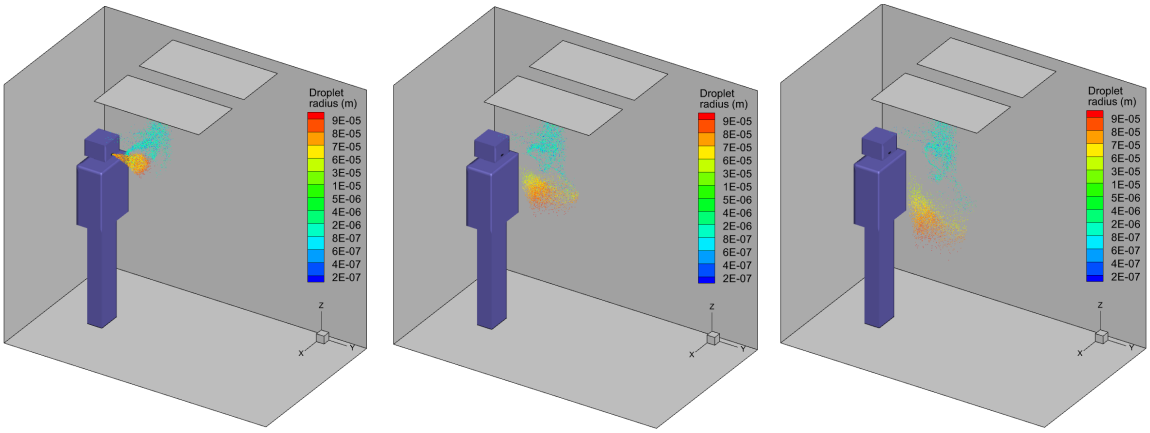

(a) Time = 7.6 s *(b) Time = 8.0 s* *(c) Time = 8.4 s*

Figure 13: Illustration of coughing at three time instances, verification case

Figure 14 is displaying the turbulent kinetic energy (TKE) in the domain, and how it is affected by the spray from a cough. A peak of the TKE can be observed in a jet shape from the moth at 7.6 second. Plot b and c displays decreased values down the line. The TKE and dissipation will be analysed further in section 4.3.

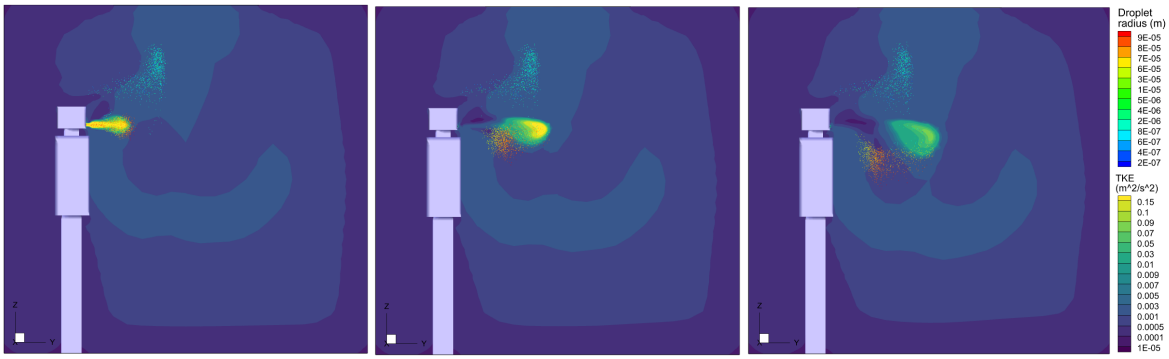

(a) Time = 7.6 s *(b) Time = 7.8 s* *(c) Time = 8.4 s*

Figure 14: The TKE countered in the domain while coughing, the verification case

3.10.3 Conclusions validation case

The results from this case illustrates the implemented method's ability to simulate the behaviour of respiratory events in an indoor environment. The combination of breathing-coughing and a cut-off evaporation function provides an opportunity to investigate the smaller airborne particles further.

The methods and results from these simulations have been submitted in a conference paper for the Scandinavian Society's conference SIMS 2022[32]. This work is done in collaboration with Ole Norbeck.

4 Results and discussion

The results from the simulations are presented in this section. Firstly, convergence and established flow pattern from the steady state simulations will be presented. Followed by a sensitivity analysis of the turbulence models. Then the flow, heat plume, droplet size distribution and among others are displayed and analysed for the cases with variation in the ACH. Lastly, a brief analysis of the two-person simulation will be presented.

4.1 Steady state

This section will give a brief analysis of the steady state simulations. As mentioned in the methodology, the results from the steady state simulations are used as input data in the transient simulations.

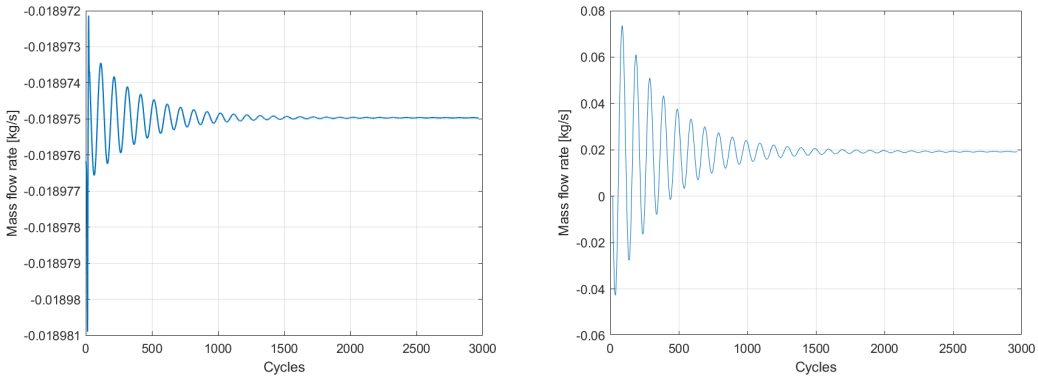

(a) Inlet *(b) Outlet*

Figure 15: Mass flow rate for the inlet and the outlet for the steady state simulation for case 1, with the realizable k-ϵ turbulence model

The steady state simulation for case 1 reach the criteria for converging after around 3000 cycles, and figure 15 illustrates that the simulations are starting to stabilize briefly after 1000 cycles. The mass flow rate at the inlet and outlet is plotted in figure 15. The mass flow rate at the inlet stabilizes around 0.0199 kg/s and the outlet 0.0192. Case 2-9 are converging between 2000 and 3000 cycles, see appendix H for the plotted mass flow rate at the inlet and outlet for these simulations.

There is a difference between the mass flow rate at the inlet and outlet of 0.0007 kg/s. This difference is probably caused by a backflow at the outlet. The backflow will not be described in detail here, but see appendix G for an illustration. The backflow around the outlet was inside the indoor environment and therefore more dominant in the early testcases. To solve the issue with the backflow, there was added a duct of 1 meter. After this adjustment of the geometry, the backflow is only appearing inside the duct. Figure 16 shows the steady flow pattern, and there is no indication that the backflow in the duct is affecting the flow pattern inside the office.

The mass flow rate at the inlet is stabilizing around 0.0199 kg/s, which corresponds with the boundary condition for air supply at 57 m^3/h.

Figure 16 illustrates the steady flow pattern in the office for all the cases. This steady flow is used as initial conditions for the transient simulations. The streamlines in the figures are coloured by the magnitude of the velocity of the flow. As the figures show, the velocity at the inlet is around 0.1 m/s, and slightly higher at the outlet. The higher velocity through the outlet can be explained by the discussed backflow in the duct.

The velocity of the stream above the person is increasing compared with the rest of the room. Most likely is velocity in this area affected by the temperature difference between the person and its surroundings, this will be discussed further in section 4.4.1.

The person in the room is clearly disrupting the flow pattern in all the cases. "Circles" of streamlines can be observed around the person in all cases. The streamlines in case 8, plot h, are not as affected as in the other cases, this may be due to the high velocity of the supply air. Plot i of case 9 displays that person number two, who is placed under the outlet, also interrupts the flow significantly.

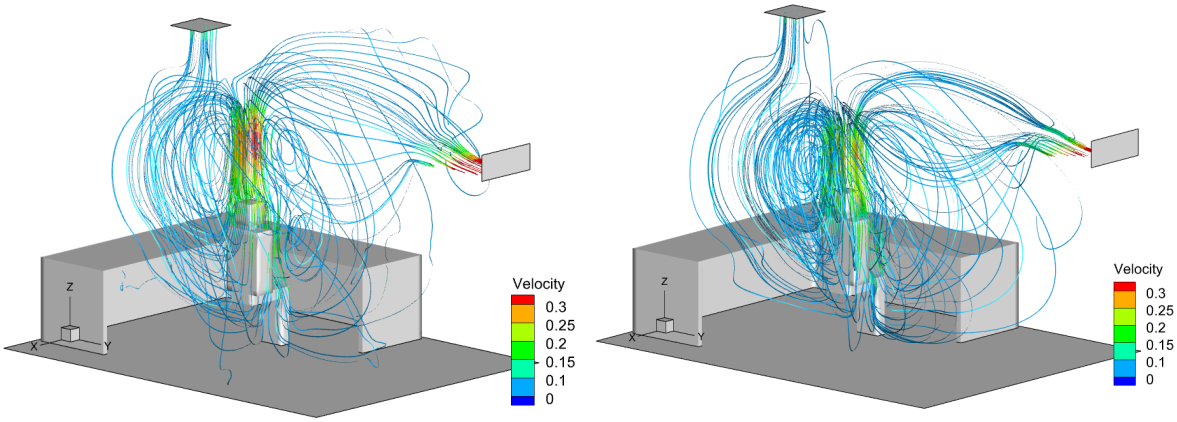

(a) Case 1, Realizable k-ϵ *(b) Case 2, Standard k-ϵ,*

Figure 16: Flow patterns, steady state

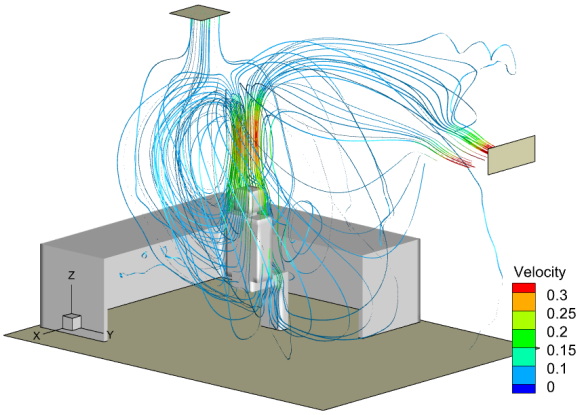

(c) Case 3, RNG k-ϵ

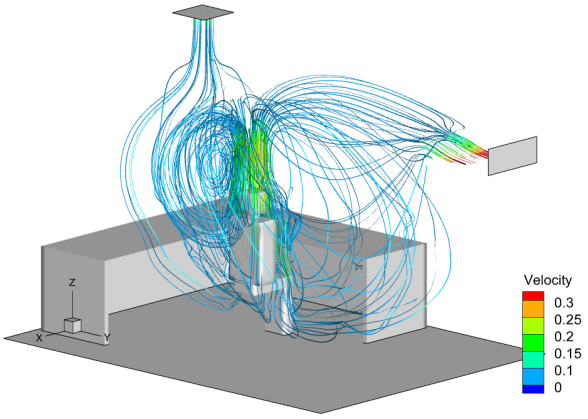

(d) Case 4, SST k-ω

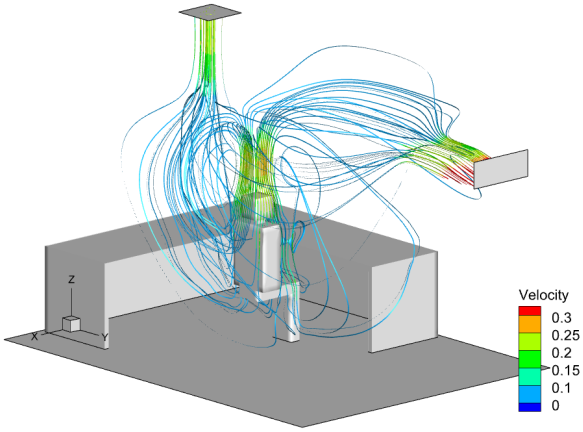

(e) Case 7, Realizable k-ϵ, $v_{supplyair}$ = 0.2 m/s

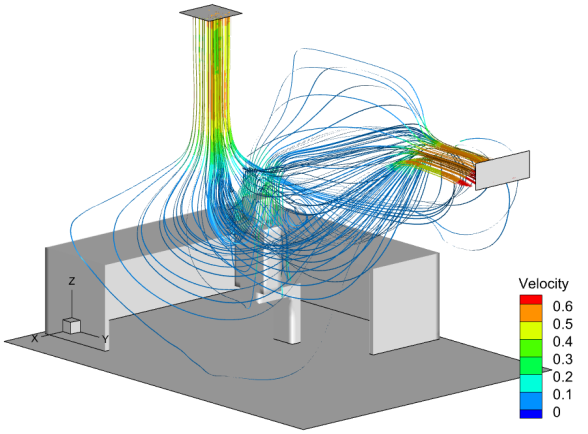

(f) Case 8, Realizable k-ϵ, $v_{supplyair}$ = 0.5 m/s

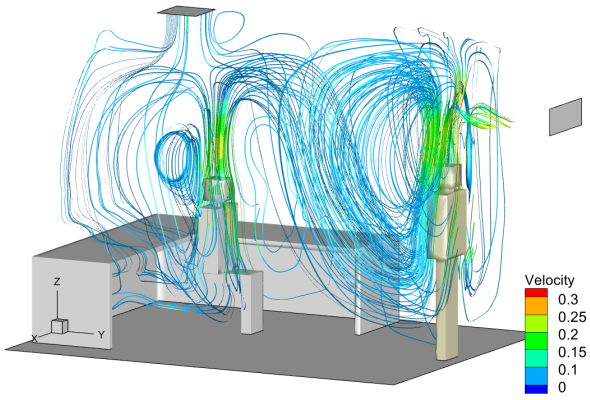

(g) Case 9, Realizable k-ϵ, two persons

Figure 16: Flow patterns, steady state

4.1.1 Yplus

The value of the y^+ are approximately 30-40 near the walls and around the person. This is in the log-layer range, and the standard wall function for the near wall treatment is therefore considered to be satisfying regarding the near wall resolution for the turbulence models.

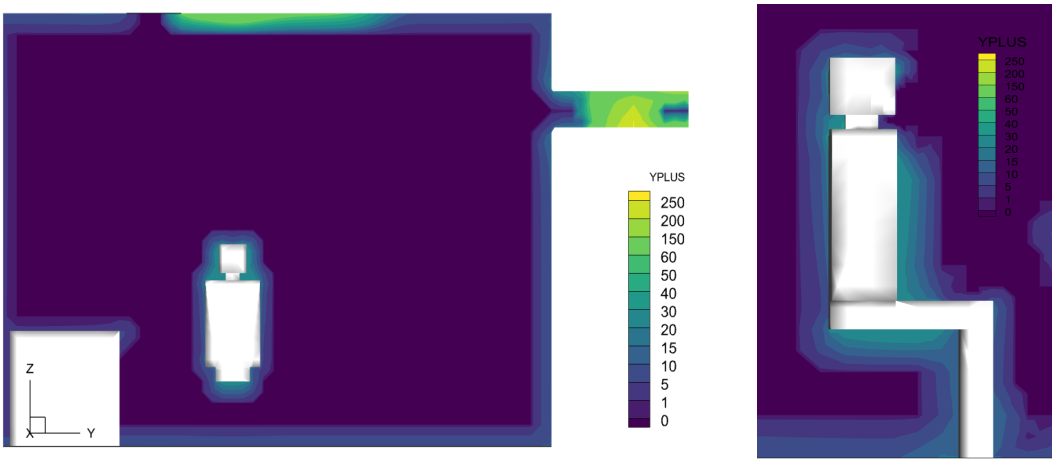

(a) y-z plane *(b) x-z plane*

Figure 17: Illustration of the y^+ in the computational domain

4.2 Adaptive Mesh Refinement

Figure 18illustrates the adaptive mesh function on a breath and a cough. The mesh is adapting the injected spray and its trajectories so that the areas with most activity have a finer grid. The time snaps of the grid resolution illustrate that the mesh is adapting quite well, and that the grid is adapting back to its original size when the particles have passed, see plot f.

The figures illustrate the mesh in 2D, but the mesh is also adapting in 3D. The droplets in the breathing and coughing sequence are coloured by droplet size, this will be described further in section 4.4.

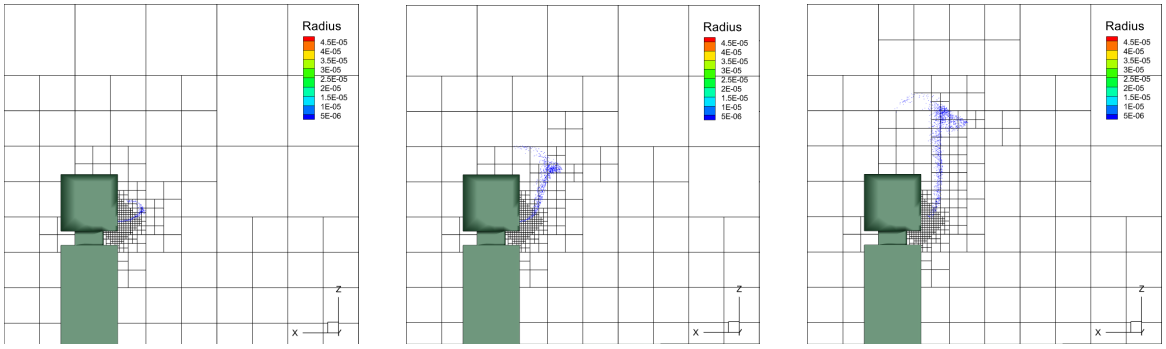

(a) time = 0.4 s *(b) time = 1.6 s* *(c) time = 2.6 s*

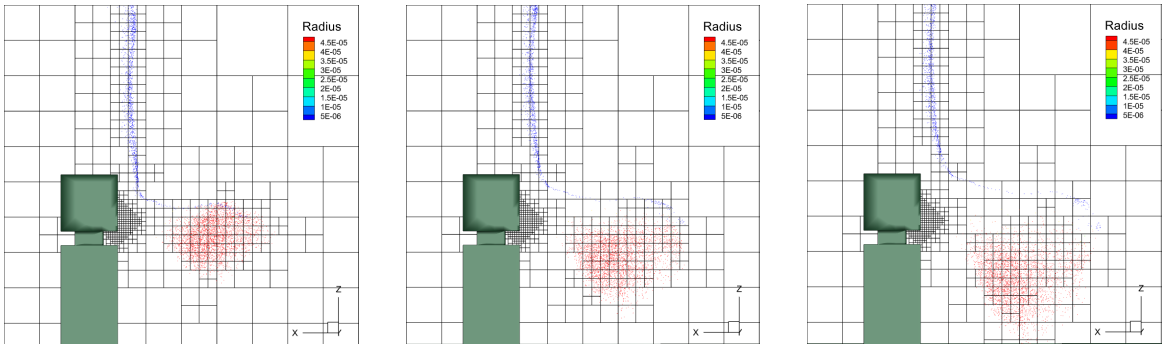

(d) time = 7.8 s *(e) time = 8.0 s* *(f) time = 8.2 s*

Figure 18: Illustration of the adaptive mesh at different times

4.3 Sensitivity analysis of the turbulence models

The results from simulation case 1-5 will be presented in this section. An analysis regarding the differences in the vector-, velocity- and turbulence field and memory usage with the chosen models is performed.

Figure 19 shows the vector field 1.8 seconds into the simulation for the four different turbulence models. All cases estimate comparable values of the velocity field. A better understanding of the predictive behaviour of these models can be analysed by looking into the detail of the jet flow region, this is shown in figure 20.

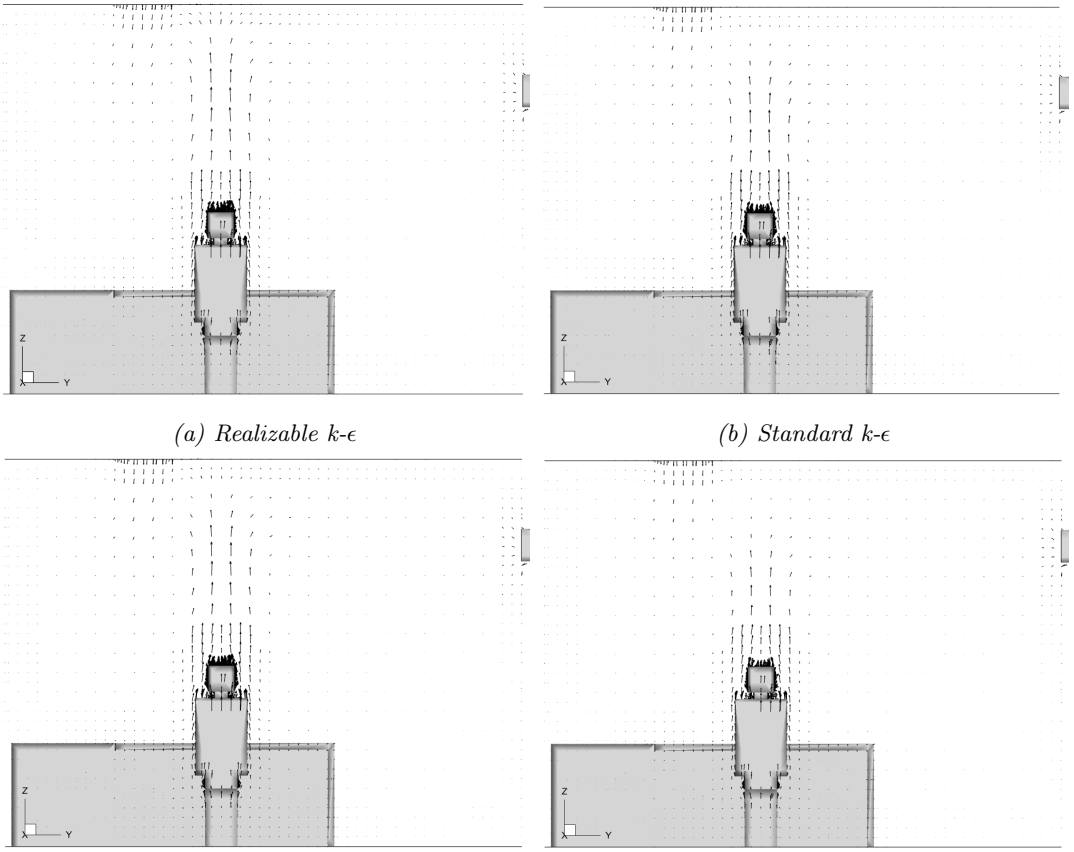

(a) Realizable k-ϵ *(b) Standard k-ϵ*

(c) RNG k-ϵ *(d) SST k-ω*

Figure 19: t=1.8 s into a breath

Three velocity profiles, at t =7.6 seconds, in streamwise direction for case 1-4 are plotted in figure 20. The profiles are numbered from profile 1 closest to the mouth, profile 2 in the middle and the last one is called profile 3. 7.6 second into the simulation corresponds to 0.09 second into the cough. The TKE in the field is contoured in the background. As can be observed from figure 20 the TKE are higher around the spray from the cough for the SST k-ω and the standard k-ϵ model.

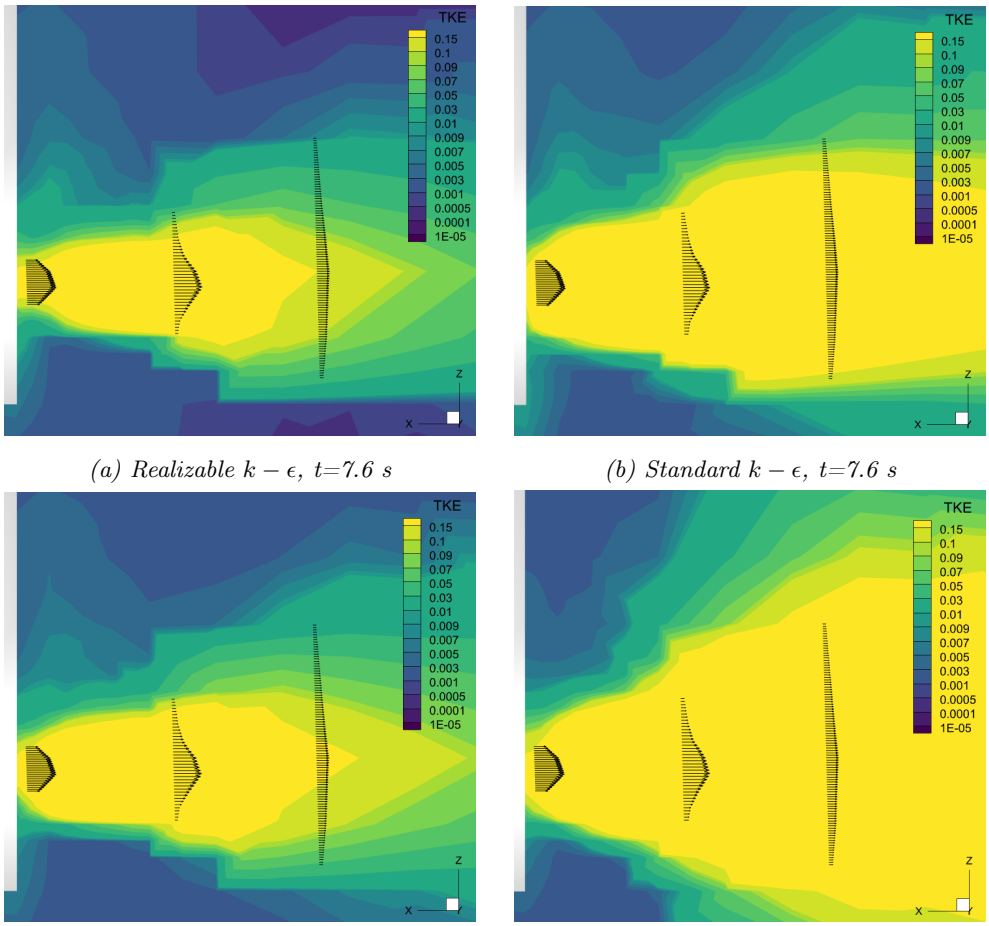

(a) Realizable $k-\epsilon$, t=7.6 s *(b) Standard $k-\epsilon$, t=7.6 s*

(c) RNG $k-\epsilon$, t=7.6 s *(d) SST $k-\omega$, t=7.6 s*

Figure 20: Profiles of the velocity in x-direction with contour of the TKE behind

The profiles for velocity, TKE and epsilon for profile 1, 2 and 3 are plotted in figure 21. The figures are scaled so that the x-values have the same scale. Regarding the velocity profiles, the variations close to the mouth are small, almost none. In profile 2 and 3 there can be observed some variations between the models, but no significant variations are observed. Case number 5, which is the realizable k-ϵ model with buoyancy effects enabled, showed almost identical results as the realizable k-ϵ model for velocity, TKE and dissipation, and is therefore not included in further analysis. For the TKE and epsilon, the variations between the models are more noticeable. For profile 1 the standard k-ϵ model clearly has higher values for both TKE and epsilon. At the most the standard k-ϵ model has at TKE value of 0.9 m^2/s^2 and epsilon value of 120 m^2/s^3 higher than the realizable k-ϵ model. For profile 2 and 3 there is a change between the standard k-ϵ and the SST k-ω model, in these two profiles the SST model has the higher values.

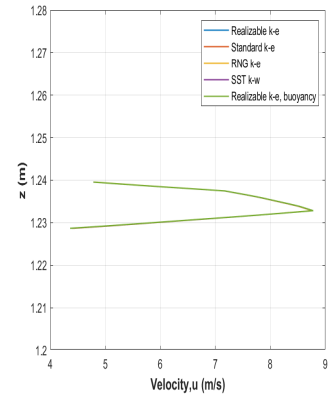

(a) Profile 1

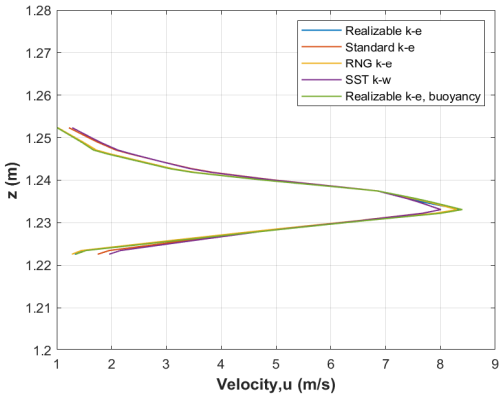

(b) Profile 2

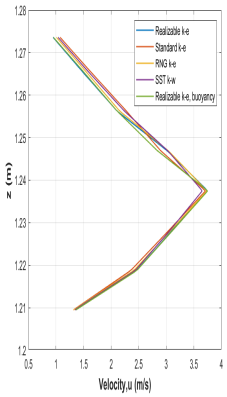

(c) Profile 3

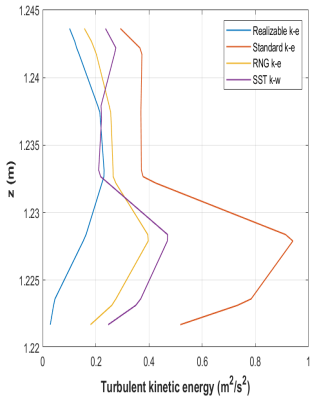

(d) Profile 1

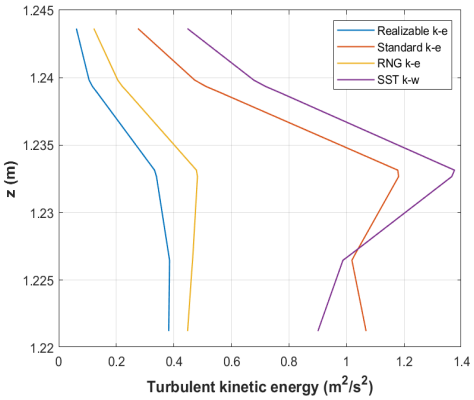

(e) Profile 2

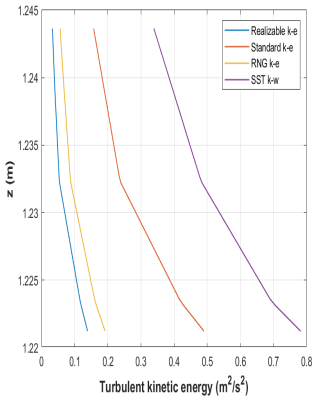

(f) Profile 3

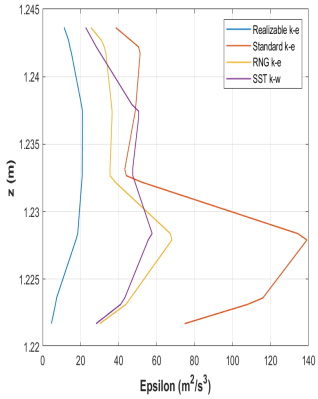

(g) Profile 1

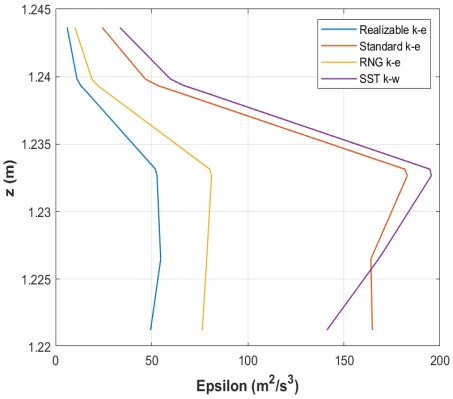

(h) Profile 2

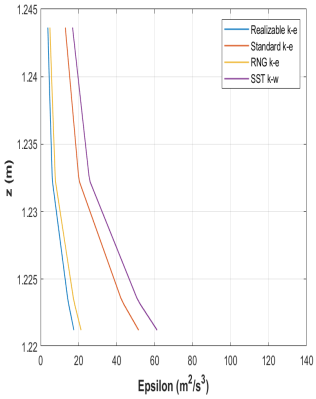

(i) Profile 3

Figure 21: The velocity profiles, TKE profiles and dissipation profiles from figure 3 plotted together in 2D

The average values for the TKE and epsilon for the whole computational domain are plotted with time in figure 22. A noticeable observation is that the SST k-ω model have significantly lower values for TKE than the k-ϵ models. The TKE in the domain have a peak after ≈ 0.5 seconds and then a barely noticeable peak around 7.5 second. One could assume that the TKE would have a higher peak at 7.5 second due to the cough. The epsilon value has peaks at the same time instances, but here the peak at 7.5 second is more noticeable. The peak for the SST k-ω model at 7.5 second is clearly higher than for the k-ϵ models.

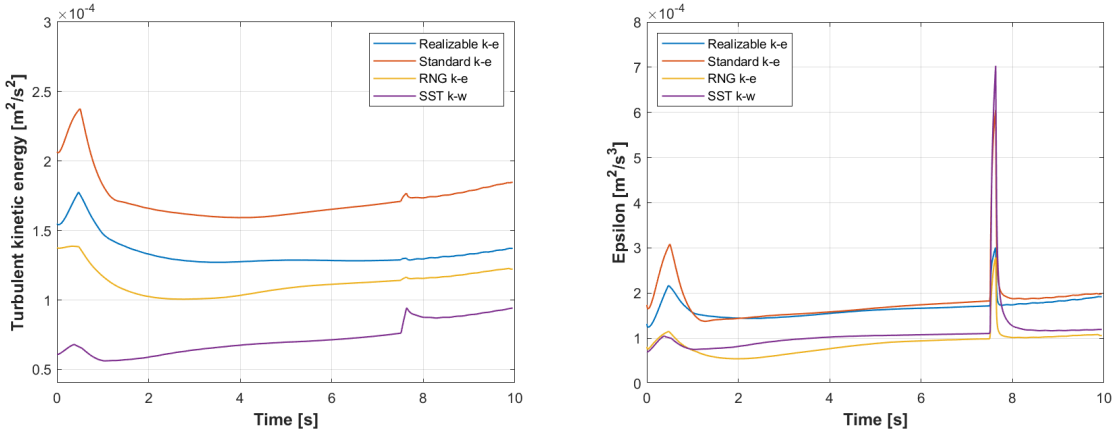

(a) TKE *(b) Epsilon*

Figure 22: The average values for the TKE and dissipation in the computation domain, case 1-4

Total number of cells in the domain and the memory usage of a simulation have a close connection. The memory usage for case 1-4 and total number of cells are plotted with time in figure 23. Plot b is the same plot as plot a, only focused on the time around the cough for better observation of the variations. The AMR creates about 1200 new cells when the person is coughing, at the same time instance, 7.5 second, the total memory usage increases from approximately 975 to 100 MB. Regarding variations between the turbulence models, there are few, observed, differences between the models.

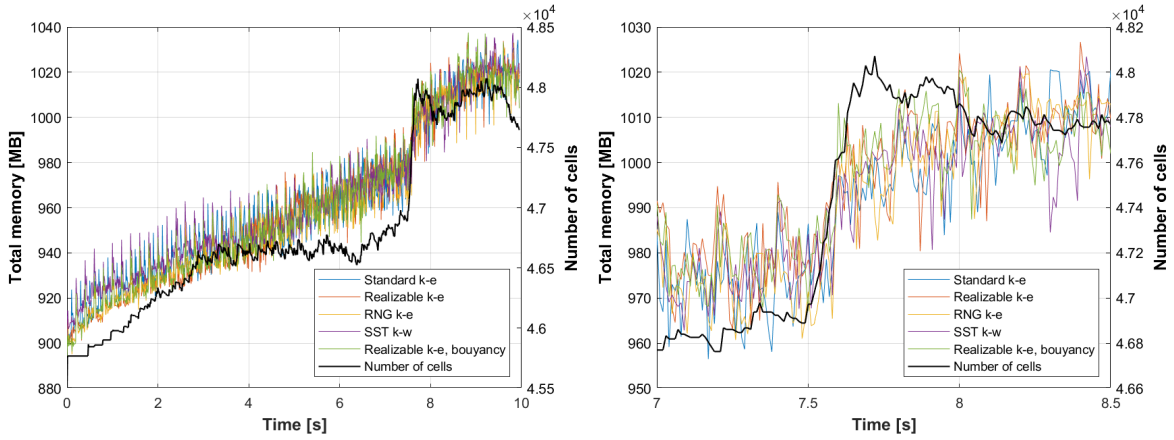

(a) From 0 to 10 secounds *(b) From 7 to 8.5 secounds*

Figure 23: Plotted memory usage and number of cells for case 1 to 5

Several authors reported the use of realizable k-e model in the literature related to Eulerian-Lagrangian approach for predicting respiratory events. From the local jet behaviour, one could see that the Realizable k-e and RNG k-e produces comparable outcomes. Additionally, no significant variations of the CPU load for these two-equations models with the present mesh resolution were observed. In the next analysis the Realizable k-e model is considered for turbulence modelling. A further analysis of the sensitivity of these models can be carried out in future with higher base grid resolution. Eventually, experimental findings would be necessary for concluding about the efficiency and performance of these models.

4.4 Evolution of the dispersed liquid phase

This section will present the results from case 6, the 60-second breathing and coughing case, with the realizable k-ϵ turbulence model. Six time instances from the simulation are plotted in figure 24 and 25. Figure 24 is a 3D presentation 1, 3 and 5 seconds of the simulation. The injected spray are coloured by droplet size. The droplets from the breathing lies in the size range 0.1 - 2.0 μg. The illustration shows that the particles are following the established flow pattern, see the displayed streamlines in figure 16a.

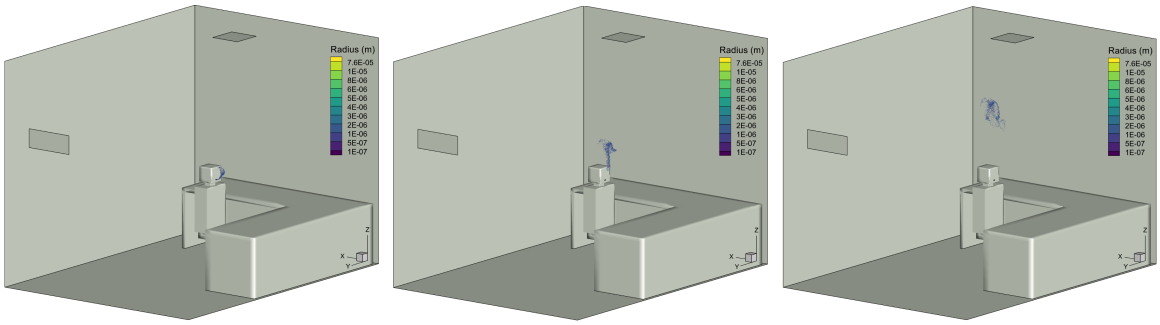

(a) time = 1.0 s *(b) time = 3.0 s* *(c) time = 5.0 s*

Figure 24: 3D presentation of the simulation during and after the first breath, case 6

Figure 25 displays three time instances right after the cough, at 7.6 s, 8.0 s, and 8.4 s. The droplets from the cough are coloured yellow and have radiuses around 76 μm. These droplets have a higher mass, and they seem to be affected by gravity and dropping towards the floor when the injection-velocity decreases.

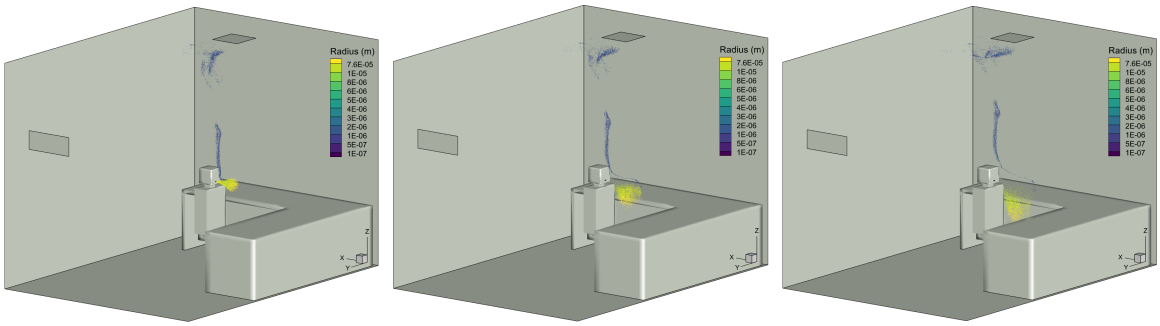

(a) time = 7.6 s *(b) time = 8.0 s* *(c) time = 8.4 s*

Figure 25: 3D presentation of the simulation right after the cough, case 6

4.4.1 Effect of thermal plume

The simulation results, plotted in figure 26, shows that the trajectories of the particles are highly influenced by natural convention due to the temperature difference between the person and the sur-

roundings. The figures are displaying the temperature field and the velocity field in the domain at the same time instances. The purpose is to highlight the connection between the velocity and the temperature. The temperature of the person is heating the surrounding air and creates a thermal plume above the person. In the area of the plume a higher velocity can be observed, between 0.1 and 0.3 m/s higher than in the rest of the domain. This phenomenon is also observed in the study Bath et al. (2022) [9], and is consistent with earlier research regarding air flow patterns and temperature differences [21], [23].

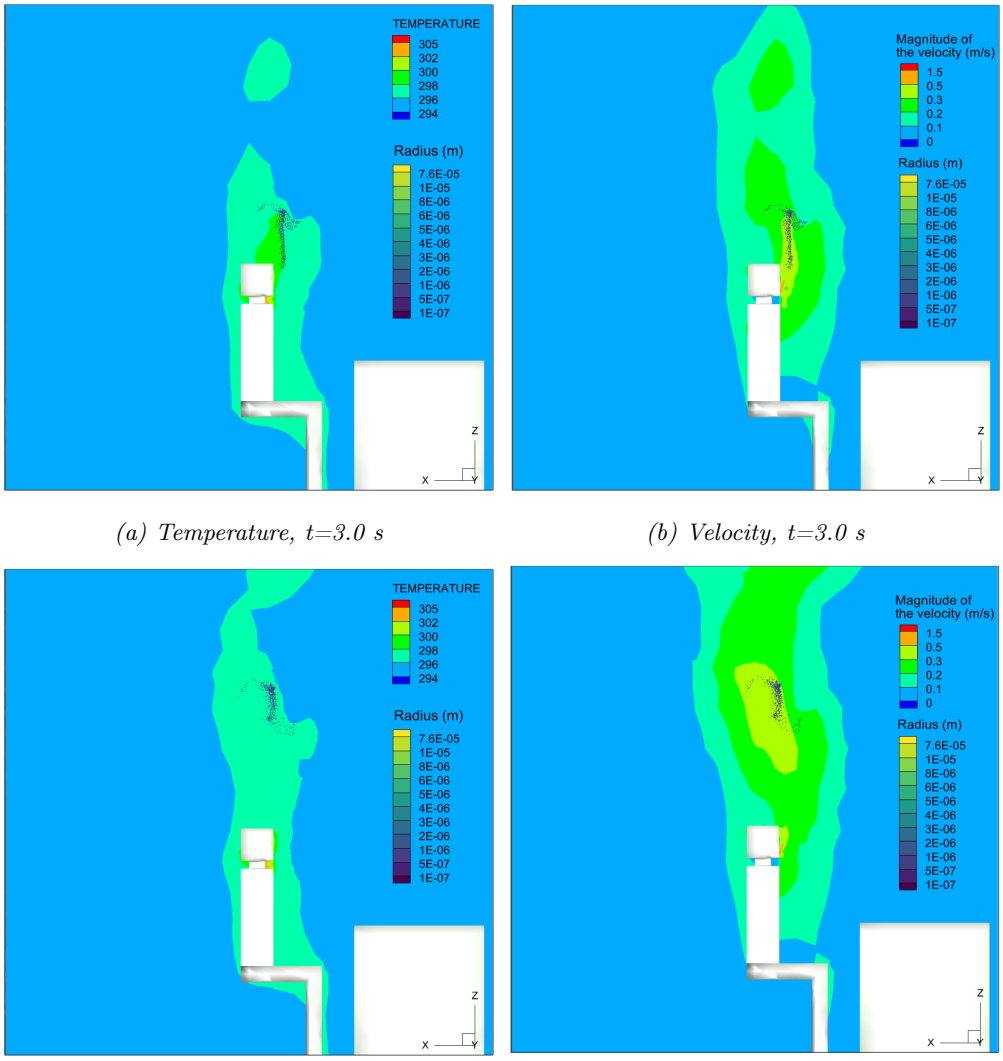

(a) Temperature, t=3.0 s *(b) Velocity, t=3.0 s*

(c) Temperature, t=5.0 s *(d) Velocity, t=5.0 s*

Figure 26: Particle motion illustrated together with the temperature and velocity, case 6

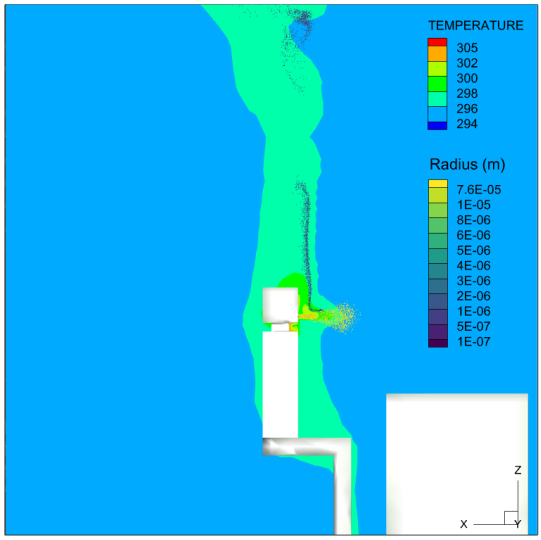

(e) Temperature, t=7.6 s

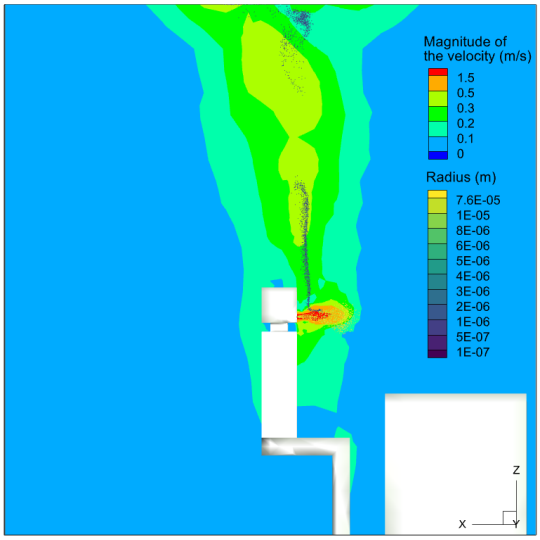

(f) Velocity, t=7.6 s

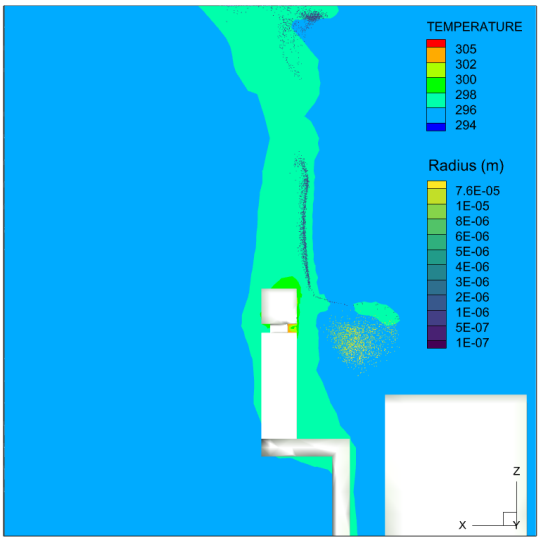

(g) Temperature, t=8.0 s

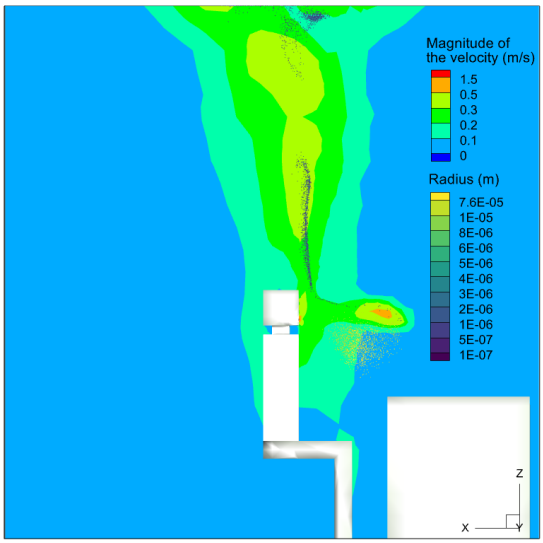

(h) Velocity, t=8.0 s

Figure 26: Particle motion illustrated together with the temperature and the magnitude of the velocity, case 6

4.5 Effect of ACH

The ACH is varied in case 6-8 by changing the velocity of the supply air. The ACH in case 6 is based on the Norwegian building regulations, and the ACH of case 7 and 8 are increased according to case 6. Figure 27 illustrates the particles at time instances, 20, 40 and 60 seconds from a side view for case 6-8 and figure 28 illustrates the same time instances from an above view.

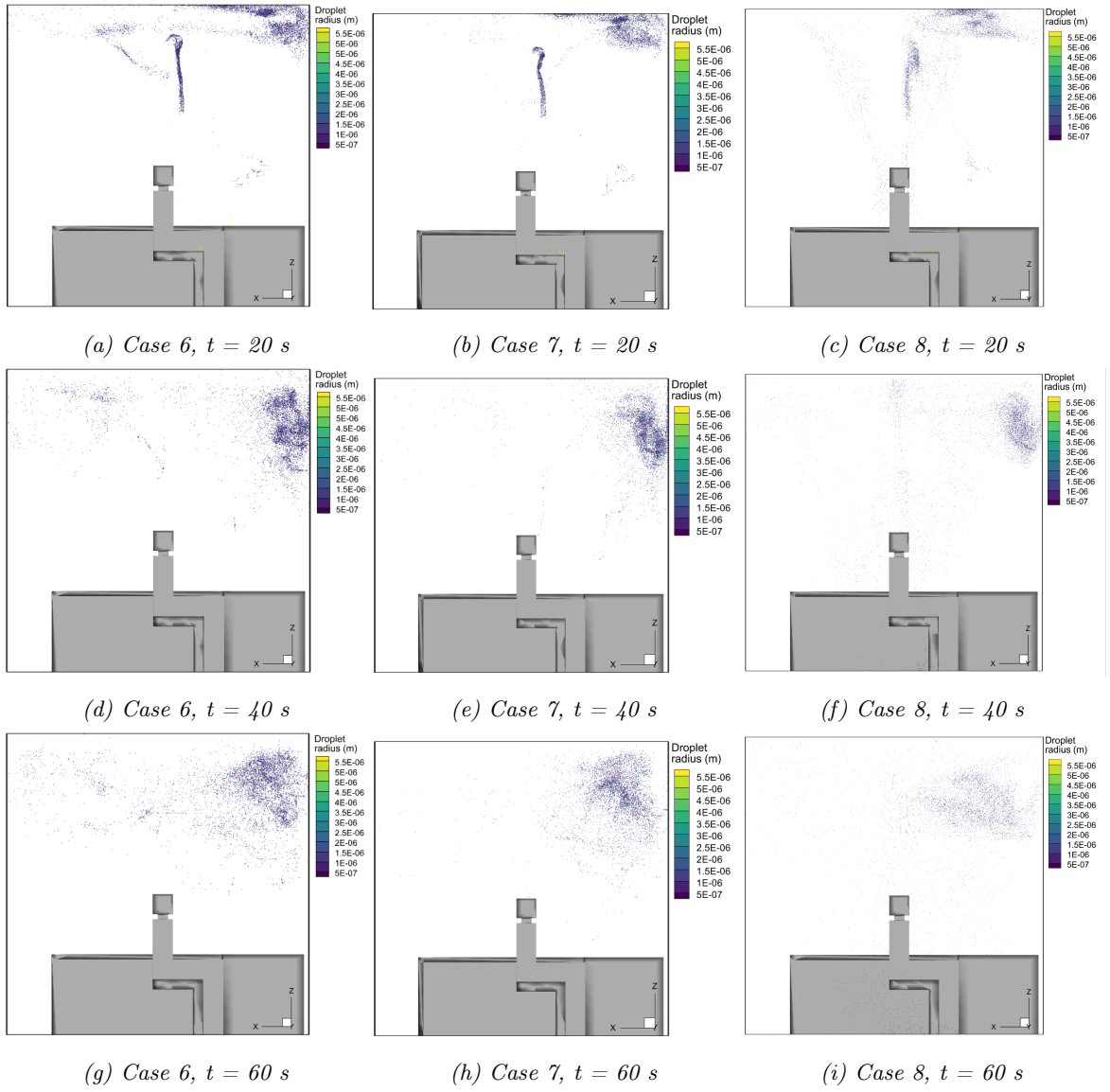

(a) Case 6, t = 20 s *(b) Case 7, t = 20 s* *(c) Case 8, t = 20 s*

(d) Case 6, t = 40 s *(e) Case 7, t = 40 s* *(f) Case 8, t = 40 s*

(g) Case 6, t = 60 s *(h) Case 7, t = 60 s* *(i) Case 8, t = 60 s*

Figure 27: Droplet pattern at different time snaps for case 6-8

The main observation from the pictures in figure 27 is the concentration of drops. The images show a clear difference in the spread of droplets. The droplets in case 7 are spreading faster than in case 6, and the droplets in case 8 are even faster spread out. Since the droplets in case 6 seem to spread out slower, the concentration of droplets in certain areas of the environment will be higher than in case 7 and 8. This indicates that the concentration of potential airborne viruses also may be higher in these areas.

The pictures in figure 28 illustrate the dispersion of the droplets from above. The plots in this figure are also showing a faster dispersion of the droplets in cases with higher ACH. It can also be noted that, based on the development in the dispersion of droplets in the room from 20 to 120 seconds, it seems like the droplets will spread out in the whole domain in all three cases with time.

Another observation that can be made from case 8 is the trajectory of the particles from the cough. The cough contains the largest particles, and is thereby coloured yellow. The yellow droplets for case 8 in plot c and f are not moving in the -x direction as they are in case 6 and 7. The droplets from the cough are moving in xy direction. If we revisit the streamlines from the steady state simulations for case 8, see figure 16f, it can be argued that the cough is being affected by the high velocity and the flow pattern from the supply air, and therefore are moving in the y-direction.

A 3D presentation of the same time instances for the three cases is added in appendix I.1. This illustration of the results emphasize the observations regarding dissipation that are given in the paragraphs above, and gives a clear picture of how the droplet patterns are developing in the room during the simulation time.

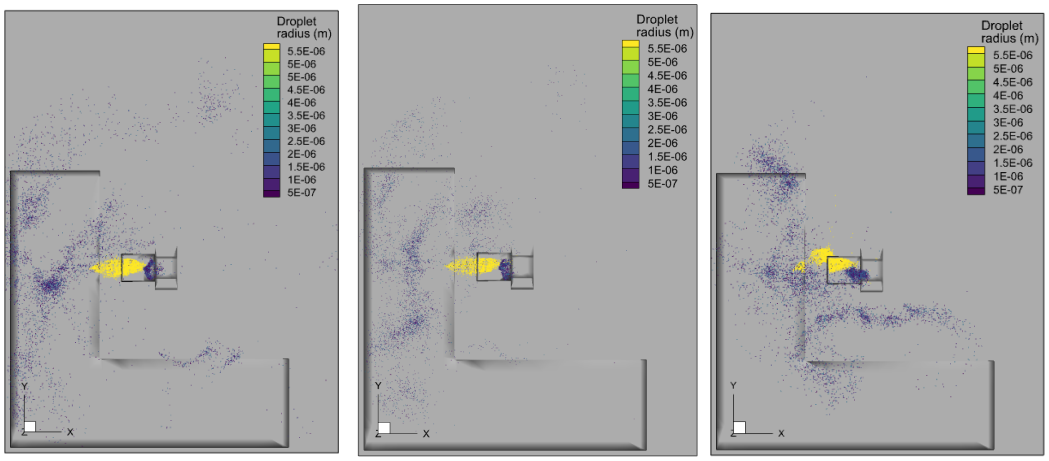

(a) Case 6, t = 20 s *(b) Case 7, t = 20 s* *(c) Case 8, t = 20 s*

Figure 28: Droplet pattern at different time snaps for case 6-8

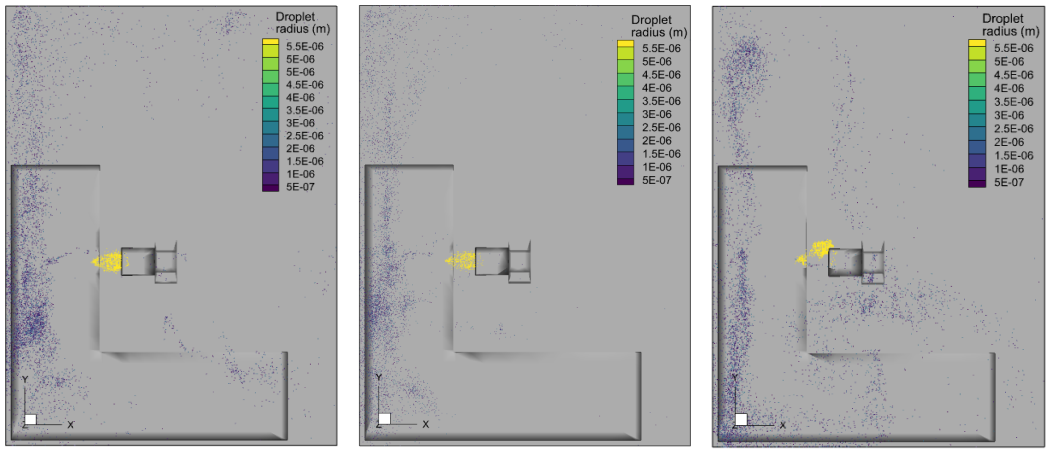

(d) Case 6, t = 40 s *(e) Case 7, t = 40 s* *(f) Case 8, t = 40 s*

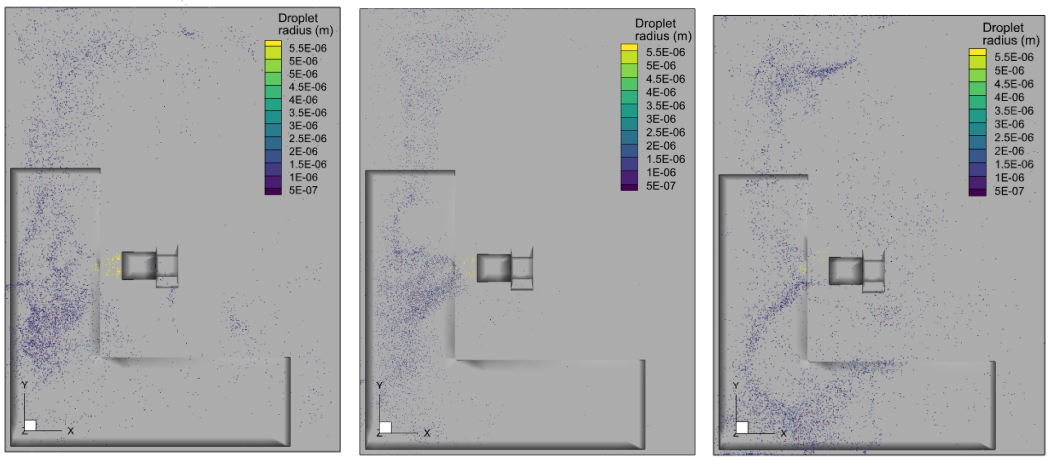

(g) Case 6, t = 60 s *(h) Case 7, t = 60 s* *(i) Case 8, t = 60 s*

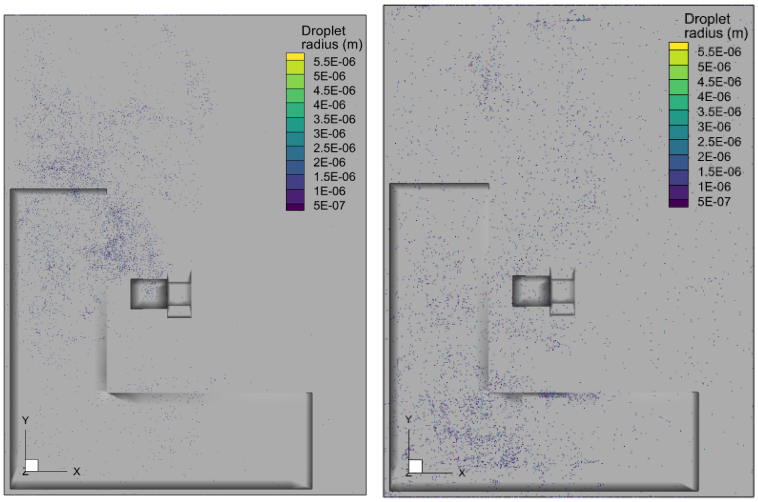

(j) Case 7, t = 120 s *(k) Case 8, t = 120 s*

Figure 28: Caption

4.5.1 Liquid phase size distribution

The droplet size distribution during the first breath is plotted for 0.6 s, 1.0 s and 1.6 s into the simulation for all three cases in figure 29. Plot a, b and c displays the size distribution for the whole computational domain, and d, e and f displays the distribution in the breathing zone. The breathing zone for a seated person is in this case defined from 1.1 to 1.7 meters above the floor. The plots of the size distribution does not show any considerable variations between the cases.

All three cases displays a high number of particles with a radius close to zero. The blue line that displays the first time instance, 0.6 s, is considerably lower than the red, 1.0 s, and yellow, 1.6 s. Most likely these particles are dived by the implemented droplet break up model, in addition will the droplets remain as very small liquid droplets and not evaporate due to the defined cut-off evaporation function.

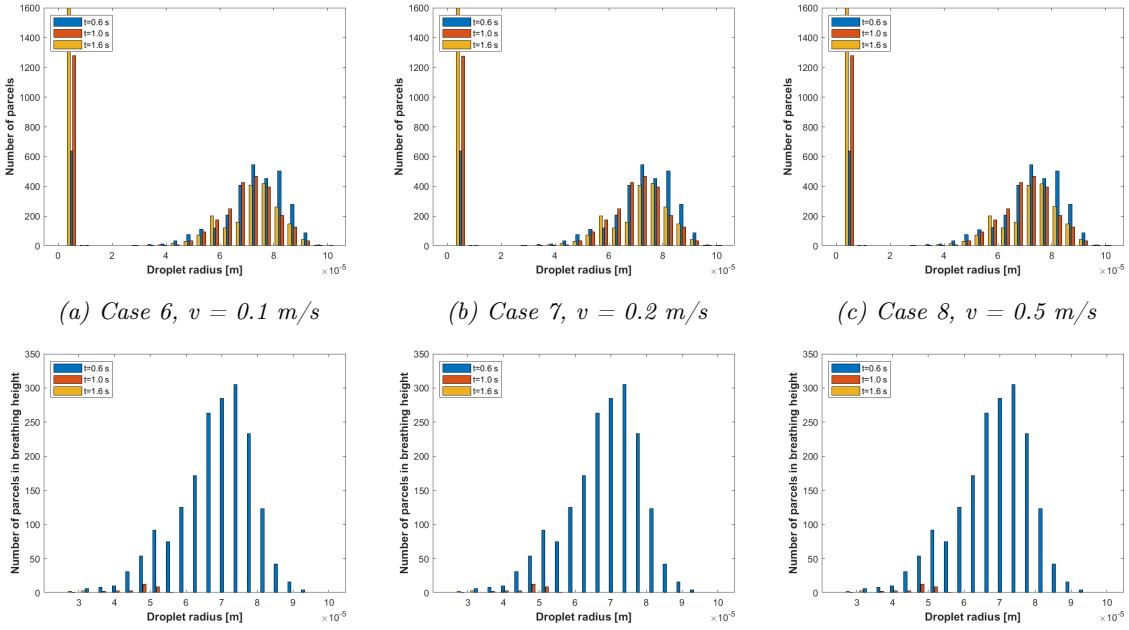

(a) Case 6, v = 0.1 m/s *(b) Case 7, v = 0.2 m/s* *(c) Case 8, v = 0.5 m/s*

(d) Case 6, v = 0.1 m/s *(e) Case 7, v = 0.2 m/s* *(f) Case 8, v = 0.5 m/s*

Figure 29: Size distribution after a breath, case 6-8

The droplet size distribution right after the cough is plotted at 7.8 s, 8.0 s and 8.4 s into the simulation in figure 30. Plot a, b and c displays the size distribution for the whole computational domain, and d, e and f displays the distribution in the breathing zone. At this time in the simulation, there is a high amount of particles with a radius close to zero in the room. To highlight the distribution of the droplets from the cough, the droplets with a radius below 10 μm have been excluded from the plots. There are some small variation between the cases, e.g. between 80 and 90 μm at 8.0 seconds. The these variations are too small to draw any conclusions from.

The distribution for the breathing zone illustrates that the droplets from coughing remains in the breathing zone for a longer time than the droplets from the breathing. This may be connected to the higher velocity and larger droplets. The "heavy" droplets will not be as much affected by the existing stream pattern in the room as the "lighter and slower" droplets from the breathing.

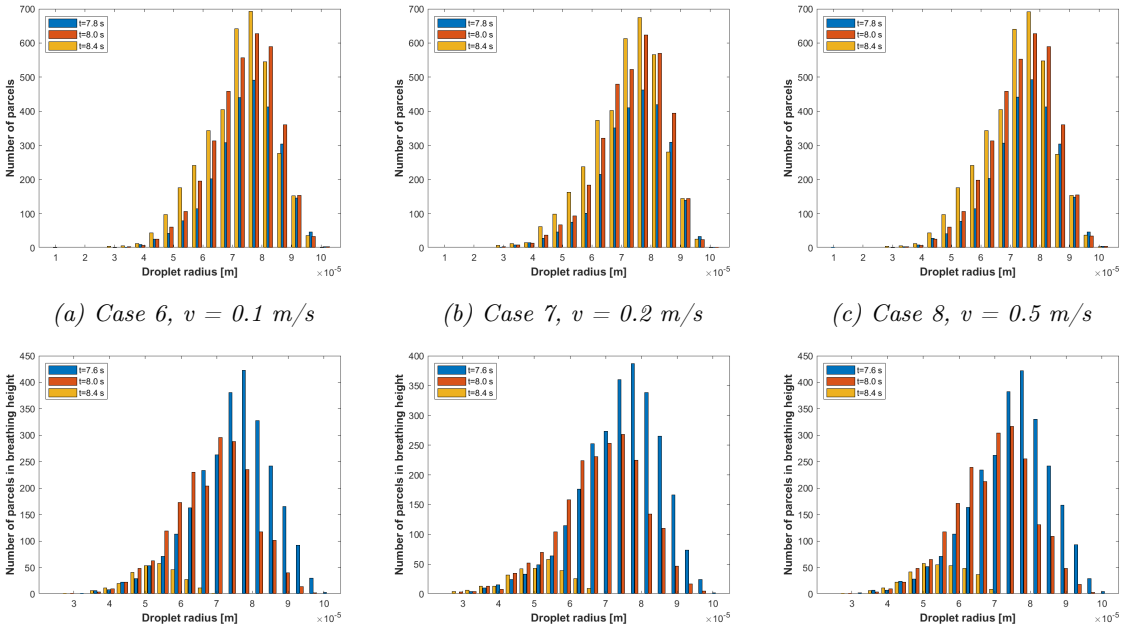

(a) Case 6, v = 0.1 m/s *(b) Case 7, v = 0.2 m/s* *(c) Case 8, v = 0.5 m/s*

(d) Case 6, v = 0.1 m/s *(e) Case 7, v = 0.2 m/s* *(f) Case 8, v = 0.5 m/s*

Figure 30: Size distribution after a cough, case 6-8

The droplet size distribution for the time instances 20, 40 and 60 seconds are plotted for the whole computational domain in figure 31. The plots show that the number of parcels with a radius around 5 μm are almost 1500 for case 6, about 750 for case 7 and 250 for case 8. The plots also displays that most particles are in the size range 0 to 5 μm after 60 seconds.

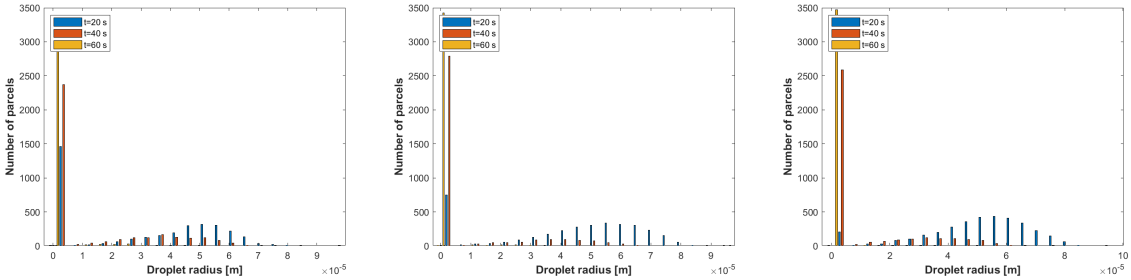

(a) Case 6, v = 0.1 m/s *(b) Case 7, v = 0.2 m/s* *(c) Case 8, v = 0.5 m/s*

Figure 31: Size distribution development, case 6-8

The spray penetration for injector one and two for case 6-8 are plotted in figure 32. The penetration is presented as a radius from the mouth, which means that the length represents the distance from the mouth to the droplets. The length is measured at the point where 95 % of the droplets have reached this distance from the mouth. The spray penetration from injector 2, which is the cough, reaches approximately 1.4 m, and does not vary between the models. The person is 1.4 m high and the gravity are affecting the droplets from the cough due to the mass. So it can be assumed that the droplets from the cough travels from the mouth toward the floor, which corresponds well with 1.4 m.

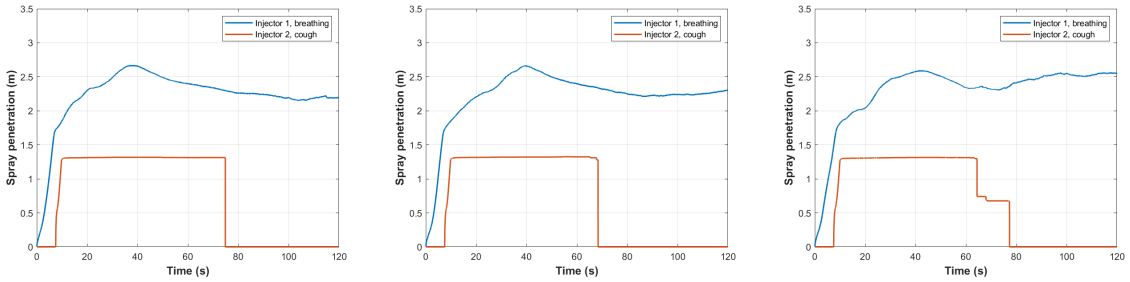

(a) Case 6, v = 0.1 m/s *(b) Case 7, v = 0.2 m/s* *(c) Case 8, v = 0.5 m/s*

Figure 32: Penetration for injector 1 and 2 for case 6, 7 and 8

The penetration for injector 1 are plotted together in figure 33. The penetration from the breathing is remarkably higher than for the cough, around 2.5 m.

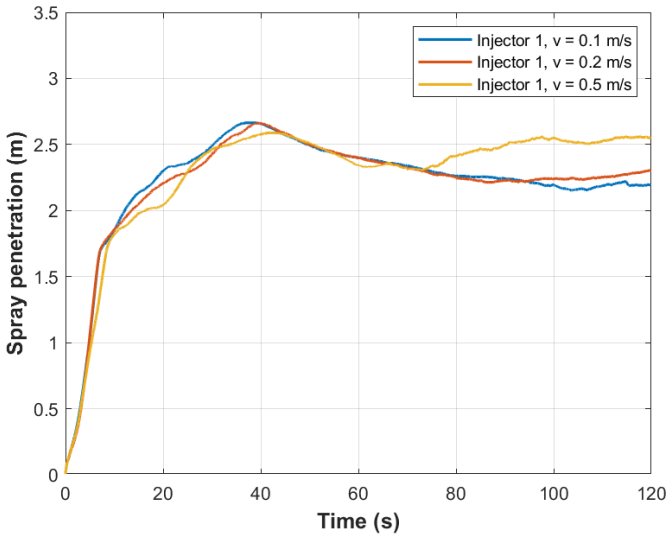

Figure 33: Penetration for injector 1 for case 6, 7 and 8

Smd, liquid mass and parcels for the three cases are plotted in figure 34. The smd reaches 80 μm which is slightly higher than the input value of 73 μm, but in accordance with the validation case. The liquid spray mass and parcels is in accordance with the input data, with a total mass around 7.7 mg (slightly higher due to breathing) and total parcels around 10 000 (four breaths and one cough). There are no major differences between the cases.

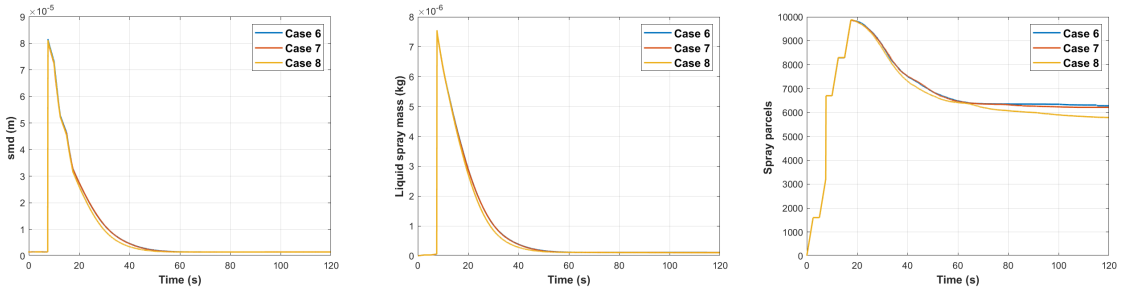

(a) smd *(b) Liquid spray mass* *(c) Liquid spray parcels*

Figure 34: Different plots regarding the injected spray in case 6, 7 and 8

The total wall film accumulation in kg is plotted in figure 35. The figure displays that case 6 and 7 have a slightly higher wall film accumulation than case 8. The film accumulation for each boundary in the domain, defined as a wall, are plotted in figure 36 and appendix I.2.

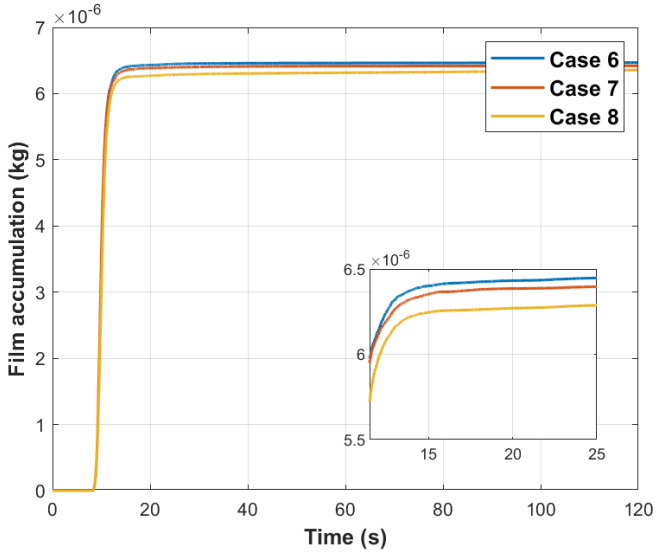

Figure 35: Total wall film accumulation in kg for case 6, 7 and 8

The wall film accumulation on the wall in front of the person is around 4 μg higher for case 6 and 7, than for case 8. A reason for the lower value in case 8 might be the flow pattern in the room.

An easy assumption is that case 8 will have the highest wall film accumulation at the wall on the right side of the person due to the characteristic flow pattern for this case, see figure 16f. It is easy to assume that the droplets will follow the flow in the y-direction and thereby hit the wall. Plot b in 36 displays that until 80 seconds into the simulation case 7 has the highest wall accumulation at this boundary.

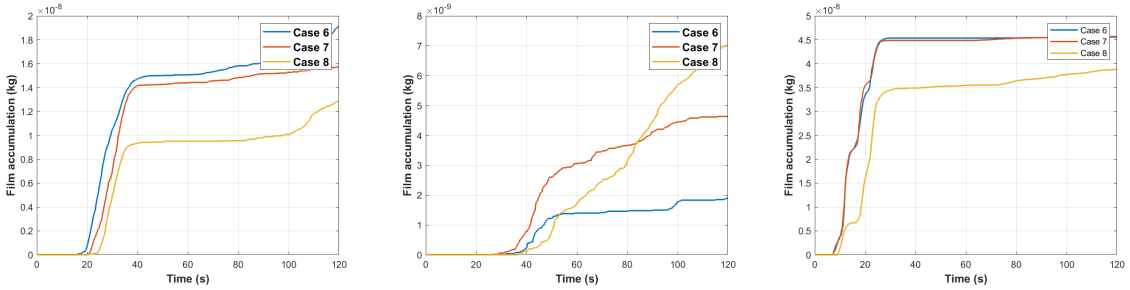

(a) Wall infront of the person *(b) Wall right side of the person* *(c) Cealing*

Figure 36: Plotted wall film accumulation for a section of boundaries in case 6-8

The behaviour and evolution of the liquid phase distribution in the room are found to be very similar for Case 6-8. However, the dispersion and spread of the liquid phase is widely different for these cases. For future analysis, it would be interesting to see how the dispersion develops over time, and observe after how long/if any of the airborne particles travels through the ventilation outlet out of the domain.

4.6 Breathing and speaking events

The last simulation case is a realistic situation in an office. It is quite normal in an office environment that one person is standing in the door talking with the person in the office. This section includes a brief analysis of the flow pattern and distribution of airborne aerosols from respiratory events in this set up.

Figure 38 and 39 the spray from the breathing, but not from the talking seams to be highly affected by the thermal plume above both persons. To analyse this further, it is added contour layers for the temperature in figure 37. In figure a and b person 1 is breathing, and the particles are clearly flowing the plume upwards, while person 2 is talking with a higher velocity, and the particles of the spray continues in the direction of the injection. In figure c and d both persons are breathing, and the particles from person two are also floating upwards.

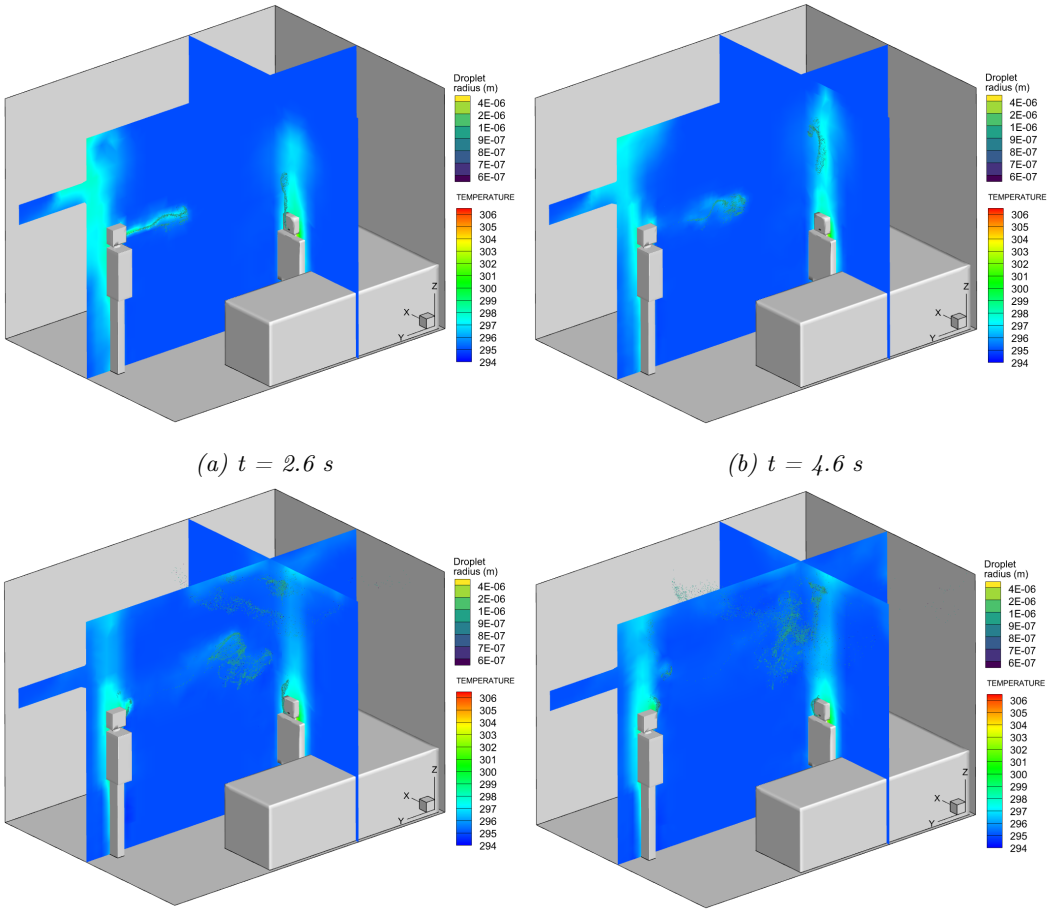

(a) t = 2.6 s *(b) t = 4.6 s*

(c) t = 12.0 s *(d) t = 16.4 s*

Figure 37: Illustration of the temperature field and trajectories of the exhaled droplets, case 9

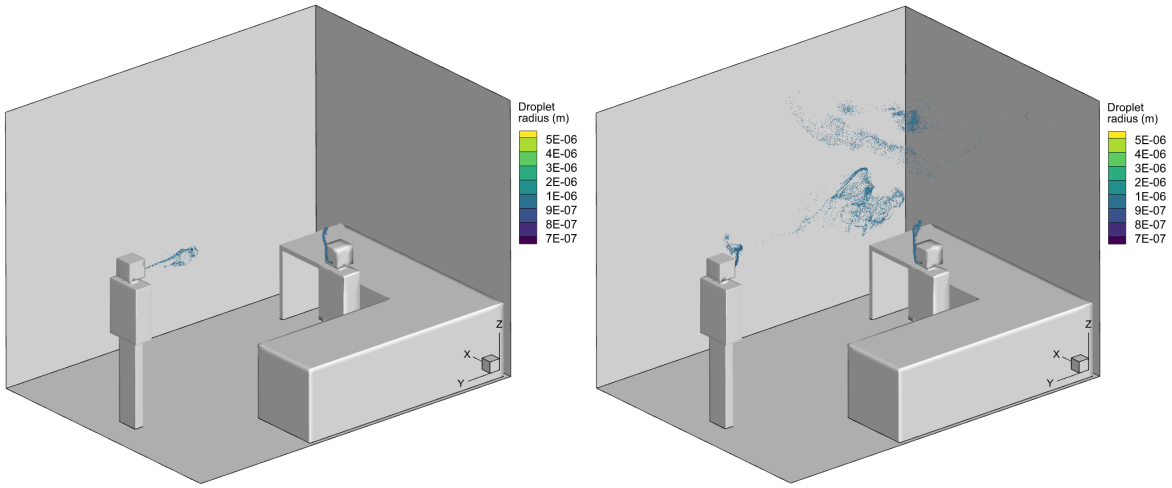

(a) t = 1.6 s *(b) t = 12.2 s*

Figure 38: Illustration of the trajectories of the exhaled droplets, case 9

Figure 39 illustrates how the dissipation of particles is developing over time. For further analysis, it would be interesting to make longer simulations.

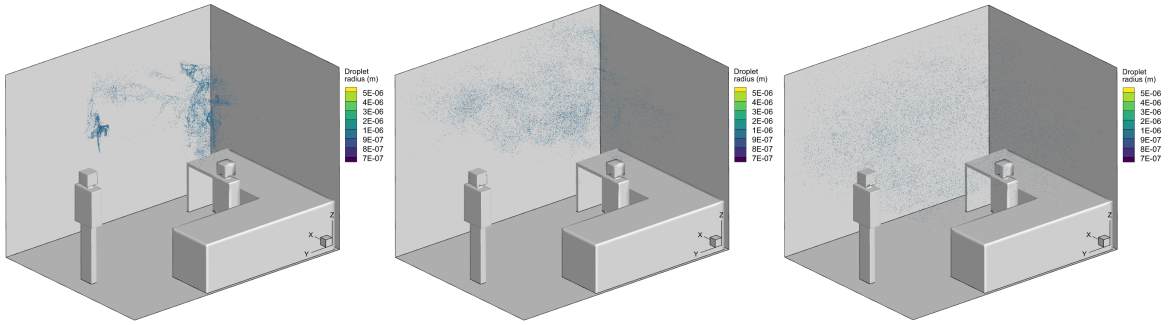

(a) t = 20 s *(b) t = 60 s* *(c) t = 120 s*

Figure 39: Illustration of the dispersion of the exhaled droplets over 120 seconds, case 9

4.7 Datapower

As discussed previously, CFD simulations can be quite complex and big, and therefore consume huge amounts of data power. Table 9 gives an overview of the consumption of cpu-hours for the simulations in this work. Appendix E gives a detailed overview of both the estimations and usage of time and data power for the most relevant test cases and the main cases from this study.

Table 9: The usage of CPU hours for each simulation

Case	**Case description**		**CPU hours**
	9 steady cases		≈ 30
Case 1	Office standard $k-\epsilon$	Breathing and coughing with UDF	110
Case 2	Office realizable $k-\epsilon$	Breathing and coughing with UDF	138
Case 3	Office RNG $k-\epsilon$	Breathing and coughing with UDF	117
Case 4	Office SST $k-\omega$	Breathing and coughing with UDF	167
Case 5	Office realizable $k-\epsilon$	With buoyancy forces enabled	-
Case 6		Velocity inlet = 0.10 m/s	-
Case 7		Velocity inlet = 0.20 m/s	-
Case 8		Velocity inlet = 0.50 m/s	-
Case 9	Two persons	Breathing and talking	475

5 Conclusion

This work aims to explore realistic scenarios of human respiratory events in an indoor environment. A FVM based 3D multiphase flow solver, with an advanced AMR function, is used to solve the compressible multi-component fluid with an Eulerian-Lagrangian approach. Since current scientific claim that particles are assumed to remain airborne with very low diameters for longer periods, a cut-off function of the evaporation when the droplet diameter becomes less than 5 μm is implemented as functions in the simulations. In addition, is a thermal difference between the person and the surroundings included in the model. The model, with the implemented cut-off function for evaporation, has been verified with a test case of a breathing-coughing sequence in a simple elevator set up.

The results include a preliminary sensitivity analysis of four different two-equation turbulence models. The results show no significantly variations between the tested models regarding velocity field and memory usage. The analysis of the local jet behaviour near the mouth displayed comparable outcomes for the Realizable k-e and RNG k-e models. The results are in accordance with the literature.

The analysis in this work shows that variation of the ACH in an indoor environment will influence the dispersion of droplets in the room. The results indicate that higher values of the ACH will disperse the droplets in the domain at a faster rate with lower ACH. This is an important aspect of is risk of infection spread through airborne particles. Furthermore, it shows how ventilation can be used as a strategy in reducing airborne transmission.

Furthermore, the implemented methods are demonstrated in a realistic scenario with two persons breathing and talking, where the dynamics of the droplets is shown and the effect from the thermal plume is illustrated. It is worth mentioning that the computational cost with the model is not too high.

The implemented model used on a realistic breathing and talking sequence together with implementation of the cut-off evaporation function and the thermal plume is a novel approach on how to gain new knowledge and understanding of the airborne viral transmission from human respiratory events in indoor environments. However, the findings in this thesis need a further investigation. Future work will involve experiments and risk analysis. These, and a couple of other, suggestion are presented in the list below.

- Experiments to validate the results
- Risk analysis of the potential risk of infection. Will droplets that contain potential infectious pathogens have the similar mass, density, evaporation rate, etc. as the modelled droplets? The concentration of infectious particles in the exhaled spray. What is the risk of infection if inhaling infectious pathogens, and how much mush the receiver inhale? These are aspects that would be interesting to investigate further.

- Longer simulation time
- Simulations with variations of the inlet temperature, together with internal heat loads, to investigate the effect the temperature of the supply air has on the flow pattern in the room.

References

[1] V. Stadnytskyi, C. E. Bax, A. Bax, and P. Anfinrud, "The airborne lifetime of small speech droplets and their potential importance in sars-cov-2 transmission," *Proceedings of the National Academy of Sciences*, vol. 117, no. 22, pp. 11 875–11 877, 2020. DOI: https://doi.org/10.1073/pnas.2006874117.

[2] N. Van Doremalen, T. Bushmaker, D. H. Morris, *et al.*, "Aerosol and surface stability of sars-cov-2 as compared with sars-cov-1," *New England journal of medicine*, vol. 382, no. 16, pp. 1564–1567, 2020. DOI: https://doi.org/10.1056/NEJMc2004973.

[3] W. F. Wells, W. Stone, *et al.*, "On air-borne infection. study iii. viability of droplet nuclei infection.," *American Journal of Hygiene*, vol. 20, pp. 619–27, 1934. DOI: https://doi.org/10.1093/oxfordjournals.aje.a118098.

[4] K. P. Fennelly, "Particle sizes of infectious aerosols: Implications for infection control," *The Lancet Respiratory Medicine*, vol. 8, no. 9, pp. 914–924, 2020. DOI: https://doi.org/10.1016/S2213-2600(20)30323-4.

[5] K. A. Prather, C. C. Wang, and R. T. Schooley, "Reducing transmission of sars-cov-2," *Science*, vol. 368, no. 6498, pp. 1422–1424, 2020. DOI: https://doi.org/10.1126/science.abc6197.

[6] P. Patrick, "Analysis of human cough in confined spaces: A numerical study," Master's Thesis, Institutt for bygg- og energiteknikk, Oslo Metropolitan University, Oslo, 2021. [Online]. Available: https://hdl.handle.net/11250/2772566.

[7] T. Dbouk and D. Drikakis, "On airborne virus transmission in elevators and confined spaces," *Physics of Fluids*, vol. 33, no. 1, p. 011 905, 2021. DOI: https://doi.org/10.1063/5.0038180.

[8] F. Arpino, G. Cortellessa, G. Grossi, and H. Nagano, "A eulerian-lagrangian approach for the non-isothermal and transient cfd analysis of the aerosol airborne dispersion in a car cabin," *Building and Environment*, vol. 209, p. 108 648, 2022. DOI: https://doi.org/10.1016/j.buildenv.2021.108648.

[9] S. P. Bhat, B. R. Kumar, S. R. Kalamkar, V. Kumar, S. Pathak, and W. Schneider, "Modeling and simulation of the potential indoor airborne transmission of sars-cov-2 virus through respiratory droplets," *Physics of Fluids*, vol. 34, no. 3, p. 031 909, 2022. DOI: https://doi.org/10.1063/5.0085495.

[10] H. Motamedi, M. Shirzadi, Y. Tominaga, and P. A. Mirzaei, "Cfd modeling of airborne pathogen transmission of covid-19 in confined spaces under different ventilation strategies," *Sustainable Cities and Society*, vol. 76, p. 103 397, 2022. DOI: https://doi.org/10.1016/j.scs.2021.103397.

[11] T. Dbouk and D. Drikakis, "On coughing and airborne droplet transmission to humans," *Physics of Fluids*, vol. 32, no. 5, p. 053 310, 2020. DOI: https://doi.org/10.1063/5.0011960.

[12] V. D'Alessandro, M. Falone, L. Giammichele, and R. Ricci, "Eulerian–lagrangian modeling of cough droplets irradiated by ultraviolet–c light in relation to sars-cov-2 transmission," *Physics of Fluids*, vol. 33, no. 3, p. 031 905, 2021. DOI: https://doi.org/10.1063/5.0039224.

[13] C. Y. H. Chao, M. P. Wan, L. Morawska, *et al.*, "Characterization of expiration air jets and droplet size distributions immediately at the mouth opening," *Journal of aerosol science*, vol. 40, no. 2, pp. 122–133, 2008. DOI: https://doi.org/10.1016/j.jaerosci.2008.10.003.

[14] H. Holmgren, E. Ljungström, A.-C. Almstrand, B. Bake, and A.-C. Olin, "Size distribution of exhaled particles in the range from 0.01 to 2.0 μm," *Journal of Aerosol Science*, vol. 41, no. 5, pp. 439–446, 2010. DOI: https://doi.org/10.1016/j.jaerosci.2010.02.011.

[15] F. K. Gregson, N. A. Watson, C. M. Orton, *et al.*, "Comparing aerosol concentrations and particle size distributions generated by singing, speaking and breathing," *Aerosol Science and Technology*, vol. 55, no. 6, pp. 681–691, 2021. DOI: https://doi.org/10.1080/02786826.2021.1883544.

[16] S. Asadi, A. S. Wexler, C. D. Cappa, S. Barreda, N. M. Bouvier, and W. D. Ristenpart, "Aerosol emission and superemission during human speech increase with voice loudness," *Scientific reports*, vol. 9, no. 1, pp. 1–10, 2019. DOI: https://doi.org/10.1038/s41598-019-38808-z.

[17] L. Morawska, G. Johnson, Z. Ristovski, *et al.*, "Size distribution and sites of origin of droplets expelled from the human respiratory tract during expiratory activities," *Journal of aerosol science*, vol. 40, no. 3, pp. 256–269, 2009. DOI: https://doi.org/10.1016/j.jaerosci.2008.11.002.

[18] H. Zhang, D. Li, L. Xie, and Y. Xiao, "Documentary research of human respiratory droplet characteristics," *Procedia engineering*, vol. 121, pp. 1365–1374, 2015. DOI: https://doi.org/10.1016/j.proeng.2015.09.023.

[19] X. Xie, Y. Li, H. Sun, and L. Liu, "Exhaled droplets due to talking and coughing," *Journal of the Royal Society Interface*, vol. 6, no. suppl_6, S703–S714, 2009. DOI: https://doi.org/10.1098/rsif.2009.0388.focus.

[20] J. K. Gupta, C.-H. Lin, and Q. Chen, "Characterizing exhaled airflow from breathing and talking," *Indoor air*, vol. 20, no. 1, pp. 31–39, 2010. DOI: https://doi.org/10.1111/j.1600-0668.2009.00623.x.

[21] D. N. Sørensen and L. K. Voigt, "Modelling flow and heat transfer around a seated human body by computational fluid dynamics," *Building and environment*, vol. 38, no. 6, pp. 753–762, 2003. DOI: https://doi.org/10.1016/S0360-1323(03)00027-1.

[22] S. Murakami, J. Zeng, and T. Hayashi, "Cfd analysis of wind environment around a human body," *Journal of Wind Engineering and Industrial Aerodynamics*, vol. 83, no. 1-3, pp. 393–408, 1999. DOI: https://doi.org/10.1016/S0167-6105(99)00088-4.

[23] N. Gao and J. Niu, "Cfd study on micro-environment around human body and personalized ventilation," *Building and Environment*, vol. 39, no. 7, pp. 795–805, 2004. DOI: https://doi.org/10.1016/j.buildenv.2004.01.026.

[24] K. Richards, P. Senecal, and E. Pomraning, *CONVERGE 3.0*. Convergent Science, Madison, WI, 2022.

[25] H. K. Versteeg and W. Malalasekera, *An introduction to computational fluid dynamics: the finite volume method*, 2. edition. Essex, England: Pearson Education Limited, 2007.

[26] Convergent Science. "Converge cfd software." (2022), [Online]. Available: https://convergecfd.com/.

[27] Wikipedia. "Law of the wall." (2022), [Online]. Available: https://en.wikipedia.org/wiki/Law_of_the_wall.

[28] P. J. O'Rourke and A. Amsden, "A spray/wall interaction submodel for the kiva-3 wall film model," *SAE transactions*, pp. 281–298, 2000. [Online]. Available: https://www.jstor.org/stable/44634219.

[29] t. f. e. Wikipedia. "Body surface area." (2022), [Online]. Available: https://en.wikipedia.org/wiki/Body_surface_area.

[30] Direktoratet-for-byggkvalitet. "Byggteknisk forskrift (tek17) med veiledning." (2017), [Online]. Available: https://dibk.no/regelverk/byggteknisk-forskrift-tek17//.

[31] Trimble. "Sketchup." (2022), [Online]. Available: https://www.sketchup.com/.

[32] Scandinavian Simulation Society. "Sims 2022." (2022), [Online]. Available: https://scansims.org/.

Appendix

A Calculation of mass fractions

	N	O	P	Q
5	Room temperature	T_room [°C]	22.0	Pre-defined value
6	Relative humidity	RH_room [%]	50.0	Pre-defined value
7	Molar mass H2O	Mm_H2O [g/mol]	18.015280	Pre-defined value
8	Molar mass air	Mm_air [g/mol]	28.964700	Pre-defined value
9	Room pressure	P_room [kPa]	101.325000	Pre-defined value
10	Saturated vapor pressure	P_sat [kPa]	2.644203	=6.1121*EKSP((18.678-(P5/234.5))*(P5/(257.14+P5)))/10
11	Vapor pressure	P_H20 [kPa]	1.322102	=(P6*P10/100)
12	Mole fraction vapor	ϒ_H2O	0.013048	=P11/P9
13	Mole fraction air	ϒ_air	0.986952	=1-P12
14	Mass fraction H2O	ω_H2O	0.008156	=(P12*P7)/((P12*P7)+(P13*P8))
15	Mass fraction O2	ω_O2	0.231100	=(1-P14)*0.233
16	Mass fraction N2	ω_N2	0.760744	=(1-P14)*0.767
17	Sum mass fractions		1.000000	=SUMMER(P14:P16)

Figure 40: Calculation of mass fraction in excel

B Calculation of nozzle diameter

	G	H	I	J	K	L	M	N
6	**Nozzle diameter**							
7			**Breathing**	**Cough**	**Speaking**			
8	Velocity	v [m/s]	1.00	10.00	4.00			
9	Total injected mass	m [kg]	3.30E-08	7.70E-06	3.30E-08			
10	Injection duration	d_t [s]	2.5	0.12	3.5			
11	Density	rho [kg/m^3]	1019.32	1019.32	1019.32			
12								
13	Diameter nozzle	d_nozzle [m]	4.06160E-06	8.955E-05	1.7163E-06	=ROT((H9*4)/(H11*H8*H10*3.14))		

Figure 41: Calculation of nozzle dimaeters

C Calculation of smd

	H	I	J	K	L	M
29						
30	**SMD**					
31			**Coughing**			
32	q_rr		8			
33	d_bar		80			
34	r_bar		40			
35						
36	smd		73.4	=2*J34/(EKSP(GAMMALN(1-1/J32)))		
37						

Figure 42: Calculation of smd

D Velocity liquid phase

Table 10: Boundary conditions for time and velocity for the liquid phase, case 1-8

Breathing, injector 1		**Cough, injector 2**	
Time [s]	**Velocity [m/s]**	**Time [s]**	**Velocity [m/s]**
0.00	1.00	0.00	0.00
2.50	1.00	2.50	0.00
2.51	0.00	2.51	0.00
5.00	0.00	5.00	0.00
5.10	1.00	5.10	0.00
7.50	1.00	7.50	0.00
7.51	0.00	7.51	10.00
7.63	0.00	7.63	10.00
7.64	0.00	7.64	0.00
10.00	0.00	10.00	0.00
10.01	1.00	10.01	0.00
12.50	1.00	12.50	0.00
12.51	0.00	12.51	0.00
15.00	0.00	15.00	0.00
15.01	1.00	15.01	0.00
17.50	1.00	17.50	0.00
17.51	0.00	17.51	0.00
20.00	0.00	20.00	0.00

Table 11: Boundary conditions for time and velocity for the liquid phase, case 9

Breathing, injector 1		**Speaking, injector 2**		**Breathing, injector 3**	
Time [s]	**Velocity [m/s]**	**Time [s]**	**Velocity [m/s]**	**Time [s]**	**Velocity [m/s]**
0.00	1.00	0.00	0.00	0.00	4.00
2.50	1.00	3.50	0.00	3.50	4.00
2.51	0.00	3.51	0.00	3.51	0.00
5.00	0.00	5.00	0.00	5.00	0.00
5.10	1.00	5.01	0.00	5.01	4.00
7.50	1.00	8.50	0.00	8.50	4.00
7.51	0.00	8.51	0.00	8.51	0.00
10.00	0.00	10.00	0.00	10.00	0.00
10.01	1.00	10.01	1.00	10.01	0.00
12.50	1.00	12.50	1.00	12.50	0.00
12.51	0.00	12.51	0.00	12.51	0.00
15.00	0.00	15.00	0.00	15.00	0.00
15.01	1.00	15.01	1.00	15.01	0.00
7.50	1.00	7.50	1.00	7.50	0.00
17.51	0.00	17.51	0.00	17.51	0.00
20.00	0.00	20.00	0.00	20.00	0.00

E Estimation and usage of cpu hours

Recent testcases for reference	Case description	Domain (m)	Sim. Time (s)	Twrite_post	Nodes	Processors	Projected time	Actual time (h)	CPU hours
Testcase_48_1	Without UDF, cough and breathe	Elevator	12	0.1	6	32	3	0.97	187
Testcase_48_2	Without UDF, 2 x breath	Elevator	12	0.1	3	32	3	0.952	91
Testcase 48_1	With UDF, cough and breathe	Elevator	20	0.2	3	32	4	2.93	282
Testcase_Office_steady	Steady	Office (6x4x3)		0.1	3	32	2	0.42	40
Office_UDF_Ke_standard	Standard k-e, breathing and coughing	Office (3x4x3)	20	0.2	3	32	4	1.15	110
Office_UDF_Ke_realizable	RLZ K-e, (only cough?)	Office (3x4x3)	20	0.2	3	32	4	1.43	138
Cases									
Steady_ke_standard		Office (3x4x3)	-		1	32	1	0.05	2
Steady_ke_realizable		Office (3x4x3)	-		1	32	1	0.09	3
Steady_ke_RNG		Office (3x4x3)	-		1	32	1	0.12	4
Steady_kw_SST		Office (3x4x3)	-		1	32	1	0.03	1
Office_UDF_Ke_standard	Standard k-e, breathing and coughing	Office (3x4x3)	10	0.1	3	32	3	1.15	110
Office_UDF_Ke_realizable	RLZ K-e, (only cough?)	Office (3x4x3)	10	0.1	3	32	3	1.43	138
Office_UDF_ke_RNG	RNG k-e, (only cough?)	Office (3x4x3)	10	0.1	3	32	3	1.22	117
Office_UDF_kw	SST k-w	Office (3x4x3)	10	0.1	3	32	3	1.74	167
Office_UDF_	Inlet: v = 0.15 m/s	Office (3x4x3)	120	0.2	Simulated locally at OsloMet, about 6 hours and 8 processors				
Office_UDF_	Inlet: v = 0.20 m/s	Office (3x4x3)	120	0.2	Simulated locally at OsloMet, about 6 hours and 8 processors				
Office_UDF_	Inlet: v = 0.5 m/s	Office (3x4x3)	120	0.2	Simulated locally at OsloMet, about 6 hours and 8 processors				
Office_talking	Two persons, one talking and one breathing	Office (3x4x3)	120	0.2	3	32	6	4.95	475

Figure 43: Estimation and usage of data power

F Sbatch-file

Example of the code in one of the sbatch files:

```
#!/bin/bash
# Job name:
# SBATCH - -export=RLM_ LICENSE=2765@158.36.0.78
# SBATCH - -job-name=O_kw
# SBATCH - -mem=100G
#
# Project:
# SBATCH - -account=nn8005k
#
# Wall clock limit:
# SBATCH - -mail-user=S313578@oslomet.no
# SBATCH - -mail-type=END
# SBATCH - -partition=bigmem


# Number of tasks (cores):


# SBATCH - -nodes=3 - -ntasks-per-node=32


# asks SLURM to send the USR1 signal 600 seconds before end of the time limit
#SBATCH - -signal=B:USR1@60


# Max memory usage per task:
#####SBATCH - -mem-per-cpu=3936
####SBATCH - -mem-per-cpu=4G


#SBATCH - -time=4:00:00


# define the handler function
# note that this is not executed here, but rather
# when the associated signal is sent
your_cleanup_function()

echo "function your_cleanup_function called at $ (date)"
```

```
echo $ PWD rsync -arv $ SCRATCH/O_kw /cluster/projects/nn8005k/Oda/
### touch STOP



## Set up input and output files:
tar -cvf temp.tar O_kw/
mv temp.tar $SCRATCH

cd $SCRATCH
tar -xvf temp.tar
cd O_kw/


## Set up job environment:
####source /cluster/bin/jobsetup
set -o errexit # exit on errors
set -o nounset # Treat unset variables as errors
module - -force purge


module use /cluster/projects/nn8005k/CVG/V30/Convergent_Science/Environment/modulefiles/CONVERGE
module load CONVERGE-IntelMPI/3.0.24


####export LD_LIBRARY_PATH=$LD_LIBRARY_PATH:$SCRATCH/O_kw/myudf/build


trap 'your_cleanup_function' USR1


mpirun converge-intelmpi super &
wait


rsync -arv $SCRATCH/O_kw /cluster/projects/nn8005k/Oda/


exit 0
```

G Backflow

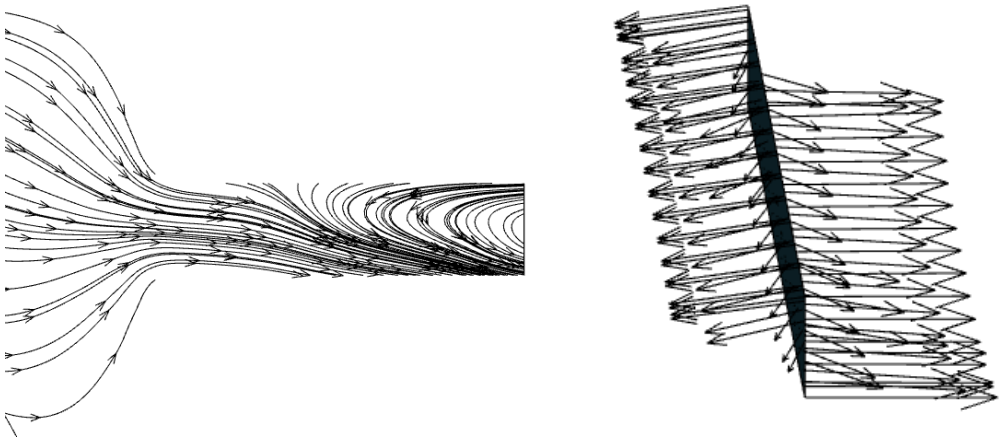

Figure 44: The streamlines and vectors that illustrates the backflow around the outlet.

H Mass flow rate, steady state

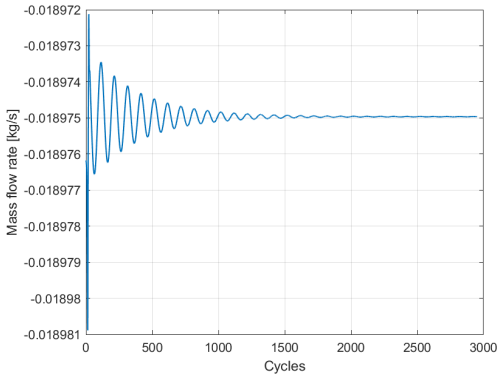

(a) Standard k-ϵ, inlet

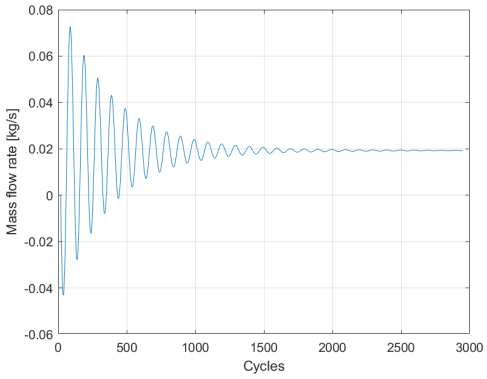

(b) Standard k-ϵ, outlet

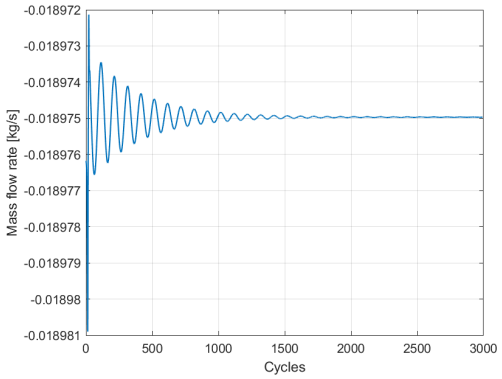

(c) RNG k-ϵ, inlet

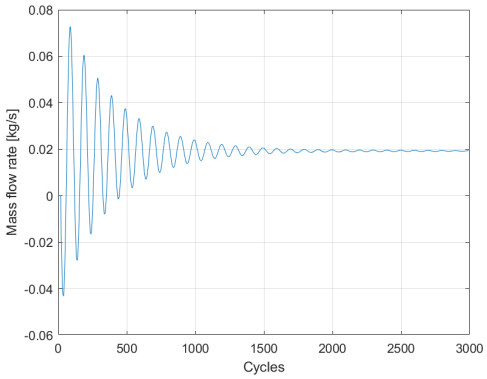

(d) RNG k-ϵ, outlet

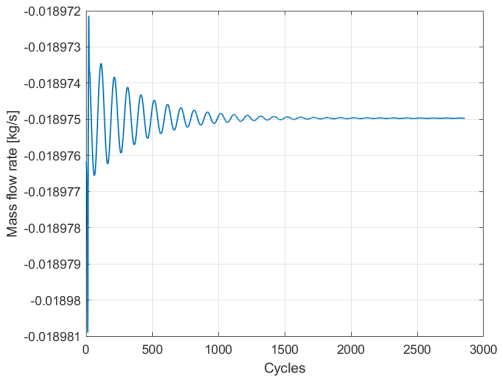

(e) SST k-ω, inlet

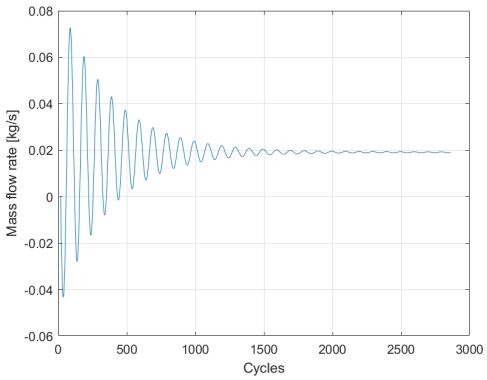

(f) SST k-ω, outlet

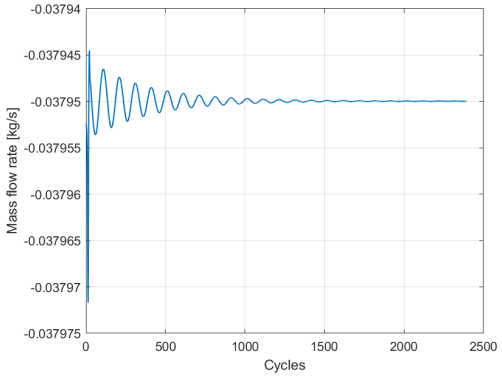

(g) velocity inlet = 0.2 m/s, inlet

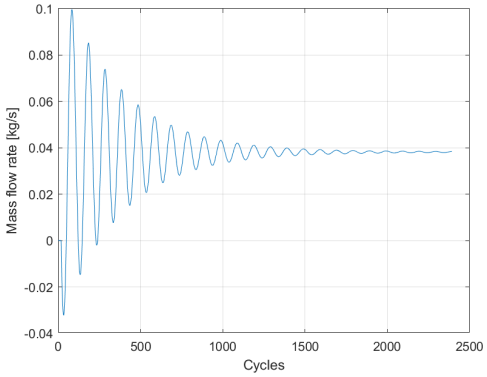

(h) velocity inlet = 0.2 m/s, outlet

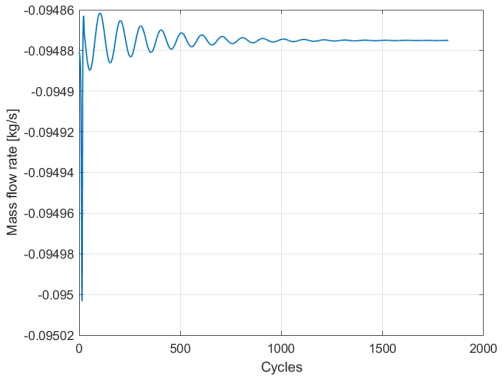

(i) velocity inlet = 0.5 m/s, inlet

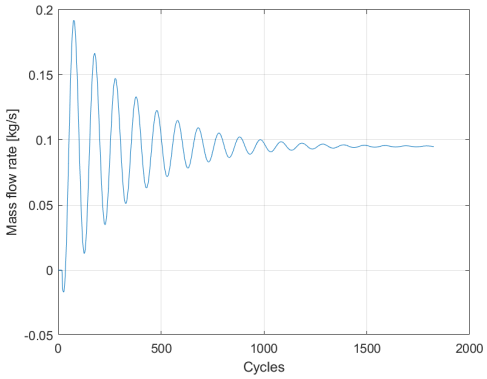

(j) velocity inlet = 0.5 m/s outlet

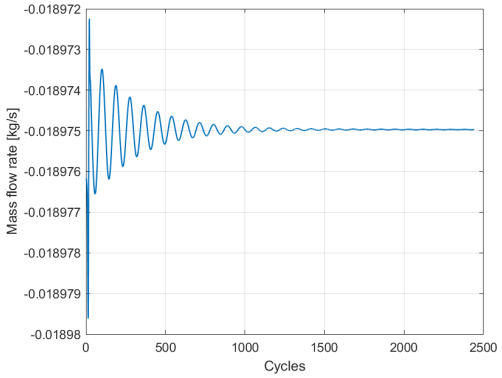

(k) Case 9, talking, inlet

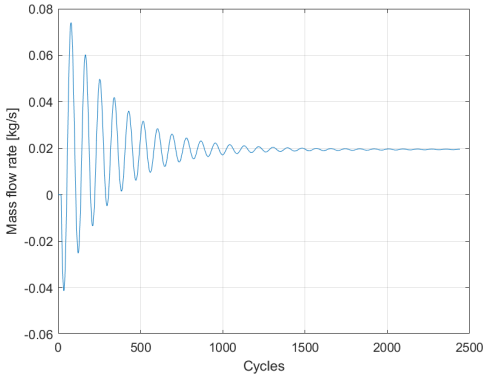

(l) Case 9, talking, outlet

Figure 45: Caption

I Variation of the ACH

I.1 Droplets

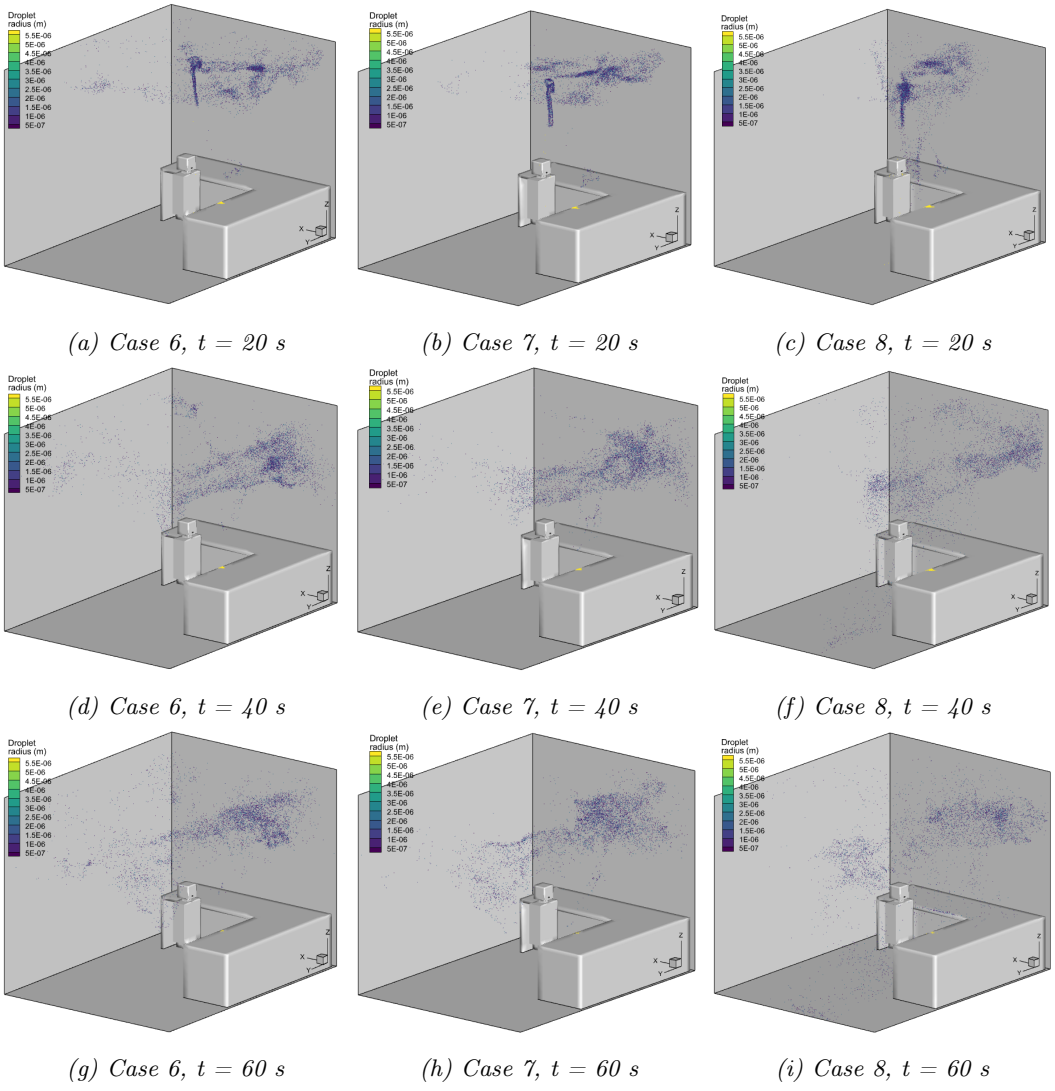

(a) Case 6, t = 20 s *(b) Case 7, t = 20 s* *(c) Case 8, t = 20 s*

(d) Case 6, t = 40 s *(e) Case 7, t = 40 s* *(f) Case 8, t = 40 s*

(g) Case 6, t = 60 s *(h) Case 7, t = 60 s* *(i) Case 8, t = 60 s*

Figure 46: Droplet pattern in 3D at different time snaps for case 6-8

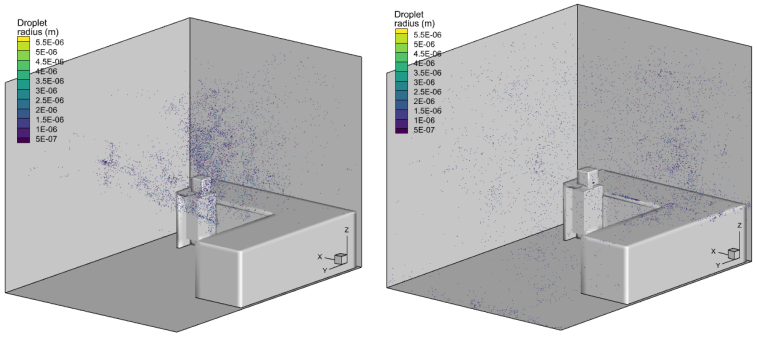

(j) Case 7, t = 120 s *(k) Case 8, t = 120 s*

Figure 46: Droplet pattern in 3D at different time snaps for case 6-8

I.2 Film accumulation at the boundaries

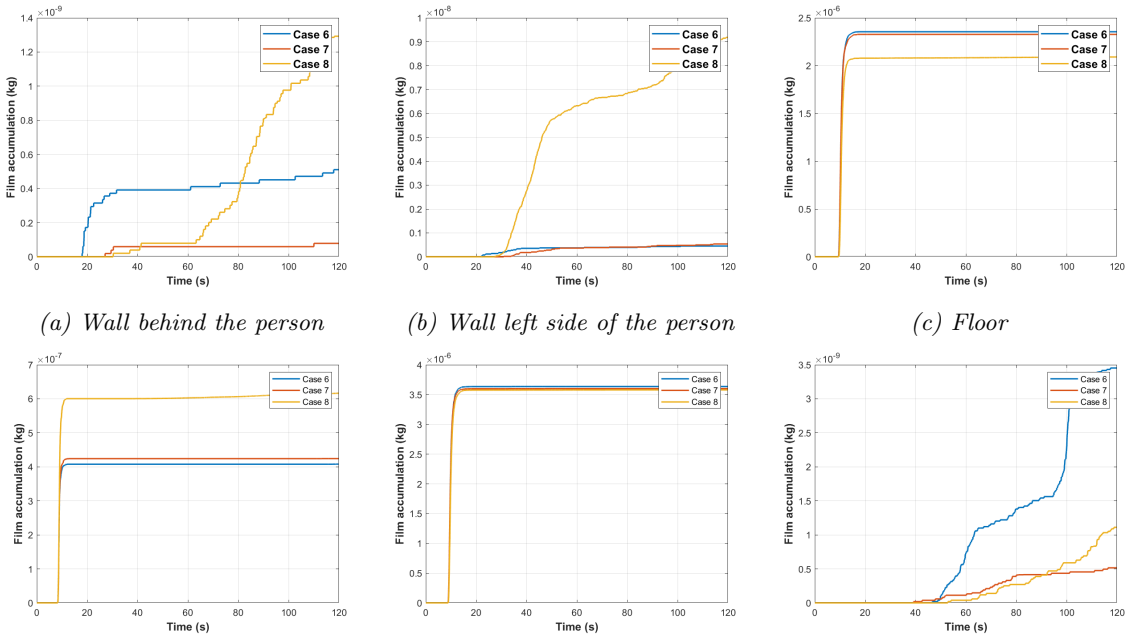

(a) Wall behind the person *(b) Wall left side of the person* *(c) Floor*

(d) Desk *(e) Person* *(f) Duckt*

Figure 47: Plotted film accumulation for a section of boundaries in case 6-8